ESTIMATING THE CONCENTRATION OF ULTRASOUND CONTRAST AGENTS USING ULTRASONIC BACKSCATTER *IN VITRO*

BY

SCOTT MICHAEL LEITHEM

THESIS

Submitted in partial fulfillment of the requirements
for the degree of Master of Science in Electrical and Computer Engineering
in the Graduate College of the
University of Illinois at Urbana-Champaign, 2011

Urbana, Illinois

Adviser:

Assistant Professor Michael L. Oelze

ABSTRACT

Ultrasound contrast agents (UCAs) are tiny microbubbles used clinically to enhance the contrast of B-mode images. Recently, UCAs have been combined with therapeutic ultrasound techniques to increase their effectiveness. These therapeutic techniques often require high concentrations of UCAs at varying pressure amplitudes, which increases the risk of adverse bioeffects. Therefore, the quantification of UCA concentration at a target location inside the body is necessary to reduce the risk of unwanted bioeffects and to determine the *in vivo* concentration of UCAs as a result of their injection. In this work, a method for extracting estimates of UCA concentration using backscatter coefficients (BSCs) was developed and verified *in vitro*. Experiments to verify the method were performed with both UCAs and glass bead microspheres in degassed water using a beaker setup and a flow system setup. Experimentally obtained estimates of the BSC were fit to ultrasound scattering models to extract concentration estimates of either the UCAs or the glass beads. The fitting was accomplished with a Levenberg-Marquardt regression algorithm, which resulted in UCA concentration and size estimates. In order to verify the estimates of UCA concentration, a sample of the UCA and degassed water mixture was extracted after the ultrasonic data were acquired, and the sample was inserted into a hemacytometer. Concentration estimates with the hemacytometer were acquired by counting the number of UCAs in a known volume of the mixture. Initial experiments with the flow system and UCAs in porcine whole blood were also conducted. The experimental BSCs of the blood by itself were compared to a calculated theoretical BSC for blood, and the experimental BSCs of the UCAs in blood were compared to experimental BSC estimates of UCAs in water. A summary of the

results is as follows. First, the estimated concentration of glass beads was within 4% of the concentration of beads flowing through the experimental flow chamber. Next, an optimal peak rarefactional pressure (PRP) amplitude range of 140-390 kPa was determined for extracting UCA concentration estimates within one standard deviation of the hemacytometer based estimates and with the UCA scattering model that was used. Finally, future investigation must focus on improving the quantification technique with UCAs in blood to be able to extract accurate concentration estimates of UCAs in blood.

ACKNOWLEDGMENTS

First, I would like to acknowledge my research advisor Dr. Michael Oelze for his ideas and support on this project. Darryl Ma must also be recognized for the previous work he did with confirming the linear relationship of UCA concentration with ultrasonic backscatter. Also, I would like to express my gratitude to Daniel King for his helpful suggestions about the models for UCA dynamics and Roberto Lavarello for his assistance with the glass bead experiments, for his suggestions for improving the experimental setup, and for his assistance with the estimation of backscatter coefficients. Finally, the support of Dr. William O'Brien Jr., the principal investigator on the grant that supported this project, must be acknowledged. This work was supported by the National Institutes of Health (NIH) grant R37EB002641.

TABLE OF CONTENTS

CHAPTER 1 INTRODUCTION

1.1 Background

Ultrasound contrast agents (UCAs) are currently used in clinical applications for enhanced imaging of blood perfused regions [1], [2], [3]. UCAs, microbubbles comprised of a gas such as air or a heavy gas such as a perfluorocarbon or nitrogen, are encapsulated by a shell of a different material. The gas has a much lower impedance than water or tissue, and so the contrast of B-mode images is enhanced. Heavy gases are utilized because they are less water soluble, which helps oppose the diffusion of the gas from the bubble, increasing the lifetime of the UCA. Perfluorocarbons are ideal for UCAs in the bloodstream because these gases have very low solubility in blood and a high vapor pressure. The shell material and thickness can vary based upon the desired application. For imaging purposes, the shell is often composed of albumin, a lipid, or a polymer with nanometer-scale thickness.

1.2 Motivation

While UCAs have been used for many years in diagnostic applications, they are not without risks. Studies both *in vivo* and *ex vivo* have been performed to validate that cavitation of UCAs can cause damage to surrounding cells and tissues [4], [5]. One early *in vivo* study [6] showed that inertial cavitation of UCAs during imaging damaged microvessels in the spinotrapezius muscle of rats. It was concluded that the level of damage was dependent upon the concentration of UCAs and the type of UCA used. Many of the *ex vivo* studies that evaluated the risk of negative bioeffects were conducted with concentrations much higher than are used clinically for imaging

purposes [7]. Also, most of these studies have reported that potential damage from the collapse of UCAs was dependent upon UCA concentration, the duration of the applied ultrasound, and the maximum pressure amplitude in the tissue.

Due to their compressibility and shell properties, UCAs have been examined for purposes other than diagnostic imaging. Therapeutic applications such as sonoporation [8], [9], sonophoresis [10], angiogenesis [11], and lithotripsy [12], [13], have been enhanced when combined with UCAs. Recently, UCAs have also been explored as a means to increase the effectiveness of tissue ablation using high intensity focused ultrasound (HIFU) [14], [15]. However, in order to improve the effectiveness of each of these techniques, a high concentration of UCAs is often required at a target location in the body. As a result, it is probable that UCAs will be present along the ultrasound pathway to the transducer focus. Nishihara et al. [16] have demonstrated that the scattering of energy and rupture of bubbles along the pathway can cause damage and disrupt the focusing of the beam. Knowledge of concentration both at the transducer focus and along the pathway to the focus is vital for minimizing damage and for optimizing the effectiveness of the UCA-enhanced therapies.

Another application of UCAs that has attracted study is their use for targeted drug delivery [17]. In using UCAs for targeted drug delivery, the drug is either inserted into the shell of the bubble or between the shell and the gas core. Once the carrier agents reach their desired destination, high intensity ultrasound is applied in order to induce inertial cavitation, releasing the drug. Eisenbrey et al. [18] showed that UCAs improved chemotherapeutic delivery to a liver tumor *in vivo* by 110%. However, it was difficult to control the amount of drug that was released because the concentration of

UCAs at the delivery site was unknown. Knowing this concentration value or devising a technique to provide estimates of the local UCA concentration would help to optimize the performance of this targeted drug delivery technique.

Thus far, because of the difficulty of knowing the dose at a target site, little work has been done to establish UCA dose versus response curves for these therapeutic techniques. Currently, UCA concentrations are estimated by the amount of prepared UCA solution inserted at the injection site. Once the UCAs have entered the bloodstream, it is estimated that 75% are lost through diffusion and fragmentation within 10 minutes [19]. Without proper knowledge of concentration levels at a specific site, it is very difficult to predict the required intensity and duration of the applied ultrasound to achieve a desired bioeffect. In addition, it becomes more difficult to conduct research to determine the optimal UCA dose for the desired bioeffects. As a result, either a technique could underperform or the risk of unnecessary damage and other undesirable bioeffects could be magnified. Therefore, it is a goal of this work to estimate UCA concentrations *in vitro* using a regression technique with the experimentally estimated backscatter coefficient (BSC) from UCAs, such that future work can assess the technique *in vivo*.

Four experiments were performed to achieve this goal. First, estimates of backscatter were obtained for UCAs in degassed water in a beaker. An *in vitro* flow system was also developed to emulate the characteristics of the dynamic environment inside the body. The second experiment consisted of obtaining backscatter estimates of glass spheres in degassed water using the flow system in order to demonstrate that the setup could be used to predict accurate scattering behavior. Third, experimental

estimates of the BSC were also obtained for UCAs in degassed water using the flow system. Finally, experimental trials were performed with UCAs in porcine whole blood using the flow system.

1.3 Literature review of BSC estimates with UCAs

In order to effectively estimate UCA concentration using backscattered ultrasound, it was necessary to utilize an appropriate theoretical model. The BSC is a powerful tool commonly used to quantify the frequency-dependent scattering of ultrasound incident upon a collection of scattering bodies. It is particularly useful because it provides a measure that is independent of system characteristics. The theoretical BSC was used to describe the scattering behavior of glass beads, UCAs, and blood. Estimates of the experimental BSC were then fit to theoretical models to extract concentration estimates of the UCAs and glass beads.

Previous estimation of the backscatter coefficient for a variety of UCAs has demonstrated that backscattered power which has been compensated for attenuation is linearly proportional to the concentration of UCAs [20], [21], [22]. This relationship was found to hold for a wide variety of frequencies, ranging from 1 to 30 MHz. One of these studies [21] found that the linear relationship held for concentrations as low as 10,000 UCAs/mL, and another [22] found that it held for concentrations as high as 20 million UCAs/mL. It is important to note that this may not be the upper limit of concentration where the linear relationship is maintained because concentrations above 20 million UCAs/mL were not investigated. In addition, the linear increase in backscattered power with concentration suggests that multiple scattering is insignificant for concentrations as high as 20 million UCAs/mL. Also, concentrations of UCAs *in vivo* may vary by location

in the body and the type of injection used. For example, for clinical imaging of the heart, a standard 2.4 mL bolus injection would be drawn into the right ventricle within a few seconds, leading to concentrations greater than 20 million UCAs/mL [20]. On the other hand, clinical perfusion imaging often utilizes a slow, constant UCA infusion technique, where UCA concentrations in tissues may remain below 200,000 UCAs/mL [20].

None of the above referenced UCA concentration studies estimated the absolute concentration of UCAs in the system based upon the resulting BSCs. Only one study [22] used the theoretical BSC from the linear model introduced in Section 2.3.1 to compare with experimental estimates. However, the concentrations of UCAs in that study were based upon the amounts inserted into the system, and no attempts were made to use experimental data to extract absolute (rather than relative) estimates. It is therefore a goal of this work to demonstrate that ultrasonic backscatter measurements can be used to estimate UCA concentrations by fitting the linear model for BSC to experimental estimates.

1.4 Organization

The thesis is organized as follows. In Chapter 2 models for the scattering of ultrasound are reviewed briefly and discussed. Chapter 3 contains a description of the methods employed to predict accurate estimates of UCA concentration using ultrasonic backscatter, as well as an explanation of the simulations. The results of the simulations and experiments are presented in Chapter 4, and Chapter 5 contains a discussion of the results and suggestions for future work.

CHAPTER 2 THEORY

2.1 Introduction

The chapter is organized as follows. Because the *in vitro* flow system was used to collect experimental BSC estimates of glass beads, the beginning of the chapter contains a short description of the theoretical scattering model for rigid spheres that was used. Next, the linear model that was used to predict UCA concentration is described (the de Jong model). A second model was also considered to describe the dynamics of UCAs that incorporates nonlinear behavior (the Marmottant model). Finally, estimates of the BSCs of UCAs in blood were obtained using the BSC of blood as a reference. For this reason, a review of the model used to predict the scattering from blood is provided in this chapter.

2.2 Scattering from glass spheres

The theoretical scattering from spherical glass beads was used to fit experimental estimates of the BSC in order to obtain estimates of glass bead size and concentration. These two parameters can be estimated using the frequency spectrum of the backscattered ultrasound from a volume of glass beads.

Briefly, the theoretical backscatter cross section for a single solid sphere (such as glass) can be calculated from the development introduced by Faran [23]. For the particular case of glass beads, the density of glass used in this work was 2.38 g/mL, the sound propagation speed was 5570 m/s, and the Poisson's ratio was 0.21. Because the backscatter cross section for a solid sphere is a function of both incident frequency and

sphere size, the characteristic size (radius) of the spheres can be determined using an optimization technique. The optimization technique used in this work is as follows [24]:

$$ESD = 2\arg\min_{R} \frac{1}{N} \sum_{i=1}^{N} \left| \mathrm{X}\left(\sigma_{BSC-\exp}(k_i), v_{Faran}(k_i, R)\right) - \bar{\mathrm{X}} \right|^2 , \qquad (2.1)$$

where

$$\mathrm{X}(u,v) = 10\log_{10}(u/v). \qquad (2.2)$$

This minimum average squared deviation technique determines the estimated scatterer diameter (ESD) using the function X, which is the ratio of the experimental BSC $\sigma_{BSC\text{-}exp}$ to the theoretical backscatter cross section of an individual solid sphere v_{Faran} in decibels. In this optimization technique k is the acoustic wavenumber, R is the radius of the glass bead, and the over-bar for X denotes the mean value of X for all k_i within the frequency bandwidth chosen for analysis.

The estimated scatterer concentration (ESC) is estimated from the ESD as [25]

$$ESC = 4\pi \frac{\sum_{i=1}^{N} \sigma_{BSC-\exp}(k_i) \cdot \upsilon_{Faran}(k_i, ESD/2)}{\sum_{i=1}^{N} \sigma_{BSC-\exp}^2(k_i, ESD/2)} . \qquad (2.3)$$

By comparing these parameters to the estimated size distribution and concentration of glass beads added to the system, the experimental flow system was validated for estimating concentrations of scattering objects.

2.3 Theoretical BSCs of UCAs

Two theoretical scattering models were studied to compare their behavior to experimental estimates. The first model was also used to develop an estimator to

estimate UCA concentration and was derived from the scattering cross section for a single UCA. The scattering cross section of an object is defined as the total acoustic power scattered by the object in all directions divided by the incident acoustic intensity [26]. In this model the UCA is assumed to oscillate linearly, and the scattering cross section does not depend upon the peak rarefactional pressure (PRP) amplitude of the incident wave.

The second model characterizes the dynamic response of a single UCA exposed to ultrasound. The model does not limit the response to linear oscillations. When the UCA oscillates nonlinearly, it does so asymmetrically; the UCA radius may expand many more times its undisturbed size while it contracts much less. In this model the response is heavily dependent upon the incident PRP amplitude.

2.3.1 Linear model

The scattering cross section of a single shelled UCA, derived from that of a single air bubble in water [27], is described by de Jong et al. [28] as

$$\sigma_{sc} = \frac{4\pi R^2}{\left(\frac{f_r^2}{f^2} - 1\right)^2 + \delta^2}, \tag{2.4}$$

where R is the resting bubble radius, f_r is the bubble resonance frequency, f is the frequency of the incident ultrasound, and δ is a damping coefficient that includes effects of re-radiation, viscosity of the surrounding fluid, and heat conduction. The damping coefficient is

$$\delta = kR + 4\frac{\eta}{p\omega r^2} + \frac{d}{b}\frac{f_r^2}{f^2}, \tag{2.5}$$

where k is the acoustic wavenumber based upon the sound speed of the suspending medium, ω is angular frequency of the applied ultrasound, η is the dynamic viscosity of the surrounding fluid, and the ratio d/b is defined in [29] and includes the effects of thermal conductivity. The resonance frequency of the bubble is [28]

$$f_r = \frac{\sqrt{\frac{S_a \beta b}{4\pi R^3 \rho} + \frac{2S_p}{\rho}}}{2\pi}, \tag{2.6}$$

where S_a is the adiabatic stiffness of the gas, β is the surface tension coefficient, S_p is called the shell parameter [30], ρ is the density of the surrounding medium, and b is the inverse polytropic coefficient. The backscatter cross section for a bubble is calculated based upon the fraction of the surface area of the transducer, A, to the total surface area of a sphere with radius equal to the distance, z_0, of the transducer to the scattering volume:

$$\sigma_{bsc} = \frac{A}{4\pi z_0^2} \sigma_{sc}. \tag{2.7}$$

If the detected ultrasound is not significantly affected by the multiple reflections of sound among the UCAs, i.e. multiple scattering is minimal, then the total backscatter coefficient is the sum of the backscatter cross section of each UCA in the resolution cell divided by its volume.

The de Jong et al. [28] model has been applied to ultrasonic backscatter results in a variety of studies in order to obtain estimates for physical parameters of multiple UCA types [31], [32], [33]. The shell friction and shell parameter estimated by [32] and [33] for Definity (Lantheus Medical Imaging Inc., North Billerica, MA) UCAs were used to calculate theoretical BSCs because these were the UCAs used in all experiments. The

surface tension at the shell-water interface was assumed to be fixed at that of water. These parameters, along with some of the physical constants that were used, are provided in Table 2.1. Also, resonant frequency versus initial UCA radius for Definity is plotted for reference in Figure 2.1.

Table 2.1 Parameters used to estimate the theoretical BSC of UCAs using the linear model

Parameter	***Symbol***	***Value***	***Unit***
Specific heat ratio for octofluoropropane	γ	1.06	-
Density of free air at sea level	P_{g0}	1.29	kg/m^3
Specific heat at constant pressure of gas	C_{pg}	1005	J/kg
Thermal conductivity of gas	K_g	0.023	W/m/°C
Surface tension at shell	τ	0.073	N/m
Dynamic viscosity of water	η	0.001	kg/m/s
Shell friction	S_f	0.015e-6	kg/s
Shell parameter	S_p	1.7	N/m

2.3.2 Nonlinear model

A model for nonlinear oscillation dynamics of UCAs was developed by Marmottant et al. [34] and was observed to match qualitatively well with experimental results of radius versus time at frequencies below 10 MHz. The model is based upon a modified Rayleigh-Plesset equation and assumes radially symmetric oscillations; thus, shear viscosity terms can be neglected. Marmottant et al. introduced a novel, varying surface tension that is a function of the instantaneous radius of the UCA.

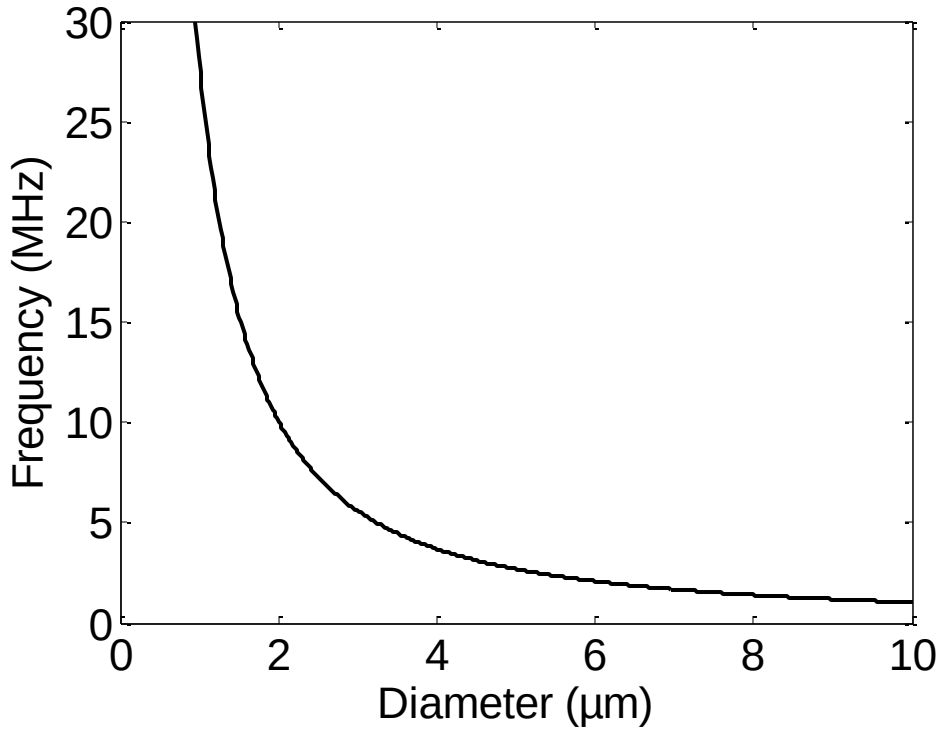

Figure 2.1 Theoretical resonance frequencies of Definity UCAs in room temperature water for varying resting diameters

The varying surface tension is defined by the state of the phospholipid monolayer shell, which can be in three different states depending upon the instantaneous radius of the UCA. At some radius, $R_{buckling}$, less than the initial radius, the shell will undergo out-of-plane buckling, and the surface tension will be effectively zero. On the other hand, when the UCA rapidly expands beyond some threshold radius, $R_{break\text{-}up}$, the monolayer will likely rupture and the resulting surface tension will relax to that of the surrounding medium. As long as $R \geq R_{ruptured}$, the surface tension will remain at that of the surrounding medium. Also, $R_{ruptured}$ is defined as the radius that the UCA will reach when the surface tension returns to that of the surrounding medium, after the initial break-up has occurred. Usually, $R_{break\text{-}up}$ is larger than $R_{ruptured}$. In between the two

threshold radii, the surface tension is characterized by a linear function of the surface area of the UCA. The final equation of motion is given by

$$\rho\left(R\ddot{R}+\frac{3}{2}\dot{R}^2\right)=\left[P_0+\frac{2\tau\left(R_0\right)}{R_0}\right]\left(\frac{R}{R_0}\right)^{-3\gamma}\left(1-\frac{3\gamma}{c}\dot{R}\right)-P_0$$

$$-\frac{2\sigma\left(R\right)}{R}-\frac{4\eta\dot{R}}{\rho R}-\frac{4\kappa_s\dot{R}}{R^2}-P_i \tag{2.8}$$

with the surface tension term

$$\tau(R)=\begin{cases}0 & \text{if } R\le R_{buckling}\\ \chi\left(\dfrac{R^2}{R_{buckling}^2}-1\right) & \text{if } R_{buckling}<R\le R_{break-up}\\ \tau_{water} & \text{if broken and } R\ge R_{ruptured}\end{cases}, \tag{2.9}$$

where R represents instantaneous radius and the dots correspond to first and second time derivatives, R_0 is initial radius, ρ is the density of the surrounding medium, γ is the polytropic gas exponent, P_0 is the ambient pressure of the medium, η is the dynamic viscosity of the surrounding medium, κ_s is the surface dilatational viscosity of the shell, P_i is the time-dependent incident pressure, χ is the elastic compression modulus that can be determined experimentally, and τ_{water} is the surface tension of the surrounding medium, about 73 dynes/cm. The physical properties of Definity UCAs that were used for the Marmottant model in this work were based upon experimental work by Goertz et al. [32] to determine κ_s and χ and are provided in Table 2.2. Note that the S_f and S_p parameters from the linear model are related to κ_s and χ by $S_f = 12\pi\kappa_s$ and $S_p = 2\chi$, respectively [35].

Table 2.2 Parameters used in the simulations to estimate the BSC with the nonlinear model

Parameter	***Symbol***	***Value***	***Unit***
Specific heat ratio for octofluoropropane	γ	1.06	-
Surface tension of water	τ_{water}	0.073	N/m
Dynamic viscosity of water	η	0.001	kg/m/s
Surface dilatational viscosity of the shell	κ_S	0.398e-9	kg/s
Elastic compression modulus of the shell	χ	0.855	N/m

With the estimates of UCA radius versus time that were obtained from Equation 2.8, the far field pressure from a spherical UCA was calculated using [35]

$$p_{ff} = \rho\left(R\ddot{R} + 2\dot{R}^2\right)\left(\frac{R}{z}\right), \tag{2.10}$$

where z is the distance between the UCA and the location of the detector. The nonlinear model for UCA dynamics was used to create a simulation which will be described in more detail in Section 3.5, and theoretical results for BSC were obtained from this simulation.

Estimation of the resonance frequency of Definity UCAs using the nonlinear model was accomplished by first estimating the far field pressure from a UCA excited with a variety of frequencies. The frequency that produced the largest scattered pressure was recorded as the corresponding resonant frequency for the UCA of fixed diameter. Note that the nonlinear model predicts a resonance frequency that is dependent upon PRP amplitude. In order to simulate the case of small amplitude oscillations using the nonlinear model, an incident PRP amplitude of 5 kPa was used to estimate the resonance frequencies. The results are presented in Figure 2.2.

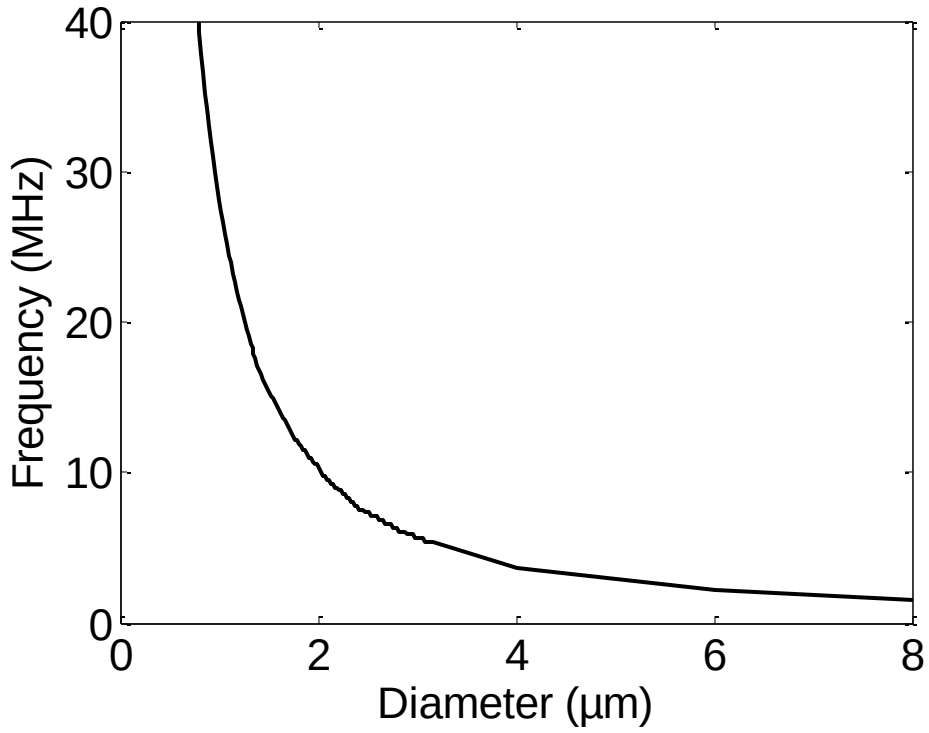

Figure 2.2 Estimated resonance frequencies of Definity UCAs in room temperature water using the theoretical model

Many studies have been performed to compare the performance of the Marmottant model to experimental data [36], [37], [38], [39]. A recent study [37] used the UCA BR-14 (Bracco S.A., Geneva, Switzerland) to compare the resonant frequencies predicted by the Marmottant model to experimentally estimated resonances under 5 MHz at peak incident pressure amplitudes below 25 kPa. They obtained good agreement with the model and concluded that the initial concentration of shell surface molecules can vary among individual UCAs, even of the same size. This is important because the concentration of surface molecules determines the initial surface tension of the shell, which is directly related to its buckling radius. In [38] and [39], the Marmottant model was used to predict the frequency response of the backscattered power of UCAs

at PRP amplitudes under 150 kPa and 6 MHz. It was concluded that the model could accurately predict the harmonics and subharmonics at low driving pressure amplitudes.

To date, however, the accuracy of the model has not been assessed at frequencies above 10 MHz. Therefore, it is a sub-aim of this work to compare the theoretical BSC simulated using the Marmottant model to experimental BSC estimates in order to evaluate the use of the model as an estimator for UCA concentration. The simulations use a 15-25 MHz Gaussian pulse to mimic the pulse from the transducer used in experiments.

2.4 Scattering from blood

The scattering of ultrasound in blood has been characterized for a wide range of frequencies, both theoretically and experimentally [40]-[46]. Although blood has many components, the red blood cells (RBCs) are by far the largest component, and it is generally accepted that the interaction with RBCs dominates the backscattered response [40]. Therefore, research has been dedicated to the analysis of ultrasound interactions with individual RBCs, suspensions of RBCs in saline, suspensions of RBCs in plasma, and whole blood. Some highlights from the key findings in each of these areas are presented here.

Single RBCs are characterized by their shape, usually referred to as a biconcave disk, where the long axis diameter is approximately 8 μm, the short axis on the outside is approximately 2 μm, and the short inner axis is 1 μm, so that the total volume is about 87 μm^3 [41]. Because the solution for a biconcave disk is not closed form, many similar shapes with closed form solutions have been proposed to approximate that of a RBC. Savéry and Cloutier [42] used the solutions for a fluid sphere, flat disk, and ellipsoid to

compare to their estimated scattering solution for a biconcave disk. Their results for the backscattering cross section of these shapes are provided in Figure 2.3. The results for O_z are for insonification along the short axis, and O_x refers to insonification along the long axis. It is important to note that below approximately 28 MHz, neither the shape nor the insonification direction affect the backscattering cross section significantly. In this work, all estimation was performed below 28 MHz, and therefore, the closed form solution for a fluid sphere was used to model the RBC.

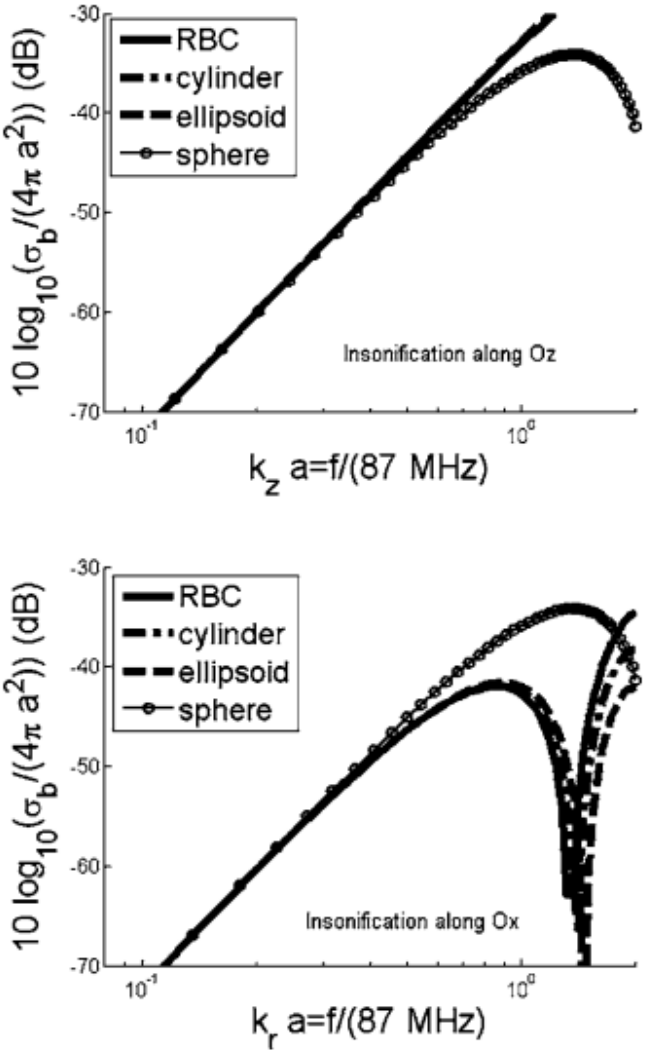

Figure 2.3 Theoretical backscattering cross sections for fluid-filled objects of varying shapes and insonification directions [42], for comparison to that of a red blood cell

Estimates of the experimental BSC of RBC suspensions in saline have been used to determine the scattering effects of blood without formation of aggregates. More specifically, the relationship of the hematocrit (the volume percentage of RBCs for a given suspension) to the BSC was examined experimentally [43]. In general, the BSC for a suspension of RBCs at very low concentrations is simply the backscattering cross section for a single RBC times the number concentration divided by the volume of the resolution cell; that is, the BSC is proportional to the number of RBCs. However, RBCs *in vivo* are at much higher concentrations, and these effects are usually grouped into a single coefficient, known as the Percus-Yevick packing factor. The closed form solution for packing factors of spheres has been derived, and usually this is used to compare experimental estimates of BSC to theoretical derivations versus hematocrit [44]. Because good agreement with theoretical estimations has been achieved for low hematocrits, these RBC-saline suspensions are often used as a reference in experiments estimating the BSCs of whole blood.

Finally, recent research in modeling the effects of whole blood aggregation on BSC has provided more accurate theoretical approximations when compared to experimental data. More specifically, a structure factor, used to describe the positions of the RBCs relative to each other, was developed, and so the BSC of whole blood is estimated by [45]

$$\sigma_{BSC-blood} = \frac{H}{V_{RBC}} \cdot \sigma_{bcs-blood} \cdot SF , \tag{2.11}$$

where H is the hematrocit, V_{RBC} is the volume of a single RBC, $\sigma_{bcs\text{-}blood}$ is the backscattering cross section of a single RBC, approximated by a sphere for frequencies

under 28 MHz, and *SF* is the structure factor, defined as the Fourier transform of the pairwise correlation function *g(r)*:

$$SF = 1 + \frac{H}{V_{RBC}} \int_r \left(g(r) - 1\right) e^{-2jkr}\, dr \approx W - \frac{12}{5}\left(Da_0\right)^2 k^2 , \qquad (2.12)$$

where *r* is the distance between two RBCs, *W* is the Percus-Yevick packing factor for a rigid sphere, *D* is the average aggregate diameter in number of RBCs, and a_0 is the radius of a sphere-shaped model for a RBC, based upon V_{RBC}. The structure factor is approximated using a second order Taylor series expansion to get the terms on the right-hand side of Equation 2.12. By fitting the experimentally estimated BSCs from RBC-plasma suspensions for varying hematocrits to this theoretical model for the BSC of blood, Yu and Cloutier [46] were able to find values for average aggregate diameter and packing factor for their data. In this way, their theoretical predictions better matched experimental BSC estimates than the models developed for RBC-saline suspensions which included the packing factor only. Because whole blood suspensions were used in the work presented in this manuscript, the model incorporating the structure factor was used for all *in vitro* experiments with blood in order to better estimate the theoretical BSC. Also, the closed-form solution of packing factor for flat disks was used in order to reduce the number of variables and approximate the shape of the RBCs.

CHAPTER 3 MATERIALS, METHODS, AND SIMULATIONS

3.1 Introduction

In the beginning of this chapter, experimental methods for estimating BSC are discussed briefly. Next, the glass beads and UCAs used in the four experiments are described. After that, a description of the methods involved for each experiment is included. Note that the beaker experiments were conducted initially because this was the simplest setup, and the flow system was developed later. Finally, the simulation used to estimate BSCs of UCAs using the nonlinear model introduced in Section 2.3.2 is explained, the results of which are presented in Chapter 4.

3.2 Experimental BSCs

3.2.1 Planar reference technique

Clinical ultrasound is most often applied in the form of B-mode imaging for diagnostic purposes [26]. In this technique, a single scan line is obtained by sending an ultrasound pulse into the tissue to be imaged and collecting the backscattered response. A B-mode image is formed by aligning adjacent scan lines to form a two-dimensional image. However, the values of each pixel in the image are dependent upon the envelope of each received scan line; thus, information about the frequency and phase of the response is discarded. Spectral-based quantitative ultrasound is the study of the frequency-dependent characteristics of the response in order to elicit tissue properties [47].

When a tissue is modeled as a collection of small particles randomly suspended in a medium, the backscattered response is treated as a linear system with a negligible coherent scattering component. Therefore, the backscattered response, neglecting frequency-dependent attenuation, is represented by

$$R_1(f) = H(f) \cdot S(f) \,, \tag{3.1}$$

where *H(f)* is the impulse response of the transducer in pulse-echo mode and *S(f)* is the total backscattering function of the medium in the frequency domain. In order to obtain information about the scattering particles, it is necessary to eliminate the transducer transfer function *H(f)*. One way that this is done is by placing a planar reference perpendicular to the propagation direction of the pulse. The scattering function of a planar surface is well defined by its acoustic reflection coefficient, a constant that is independent of frequency. Therefore, its response in the frequency domain is

$$R_2(f) = H(f) \cdot \Gamma \,, \tag{3.2}$$

where Γ is the reflection coefficient of the planar reflector. The system-independent power spectrum is calculated by taking the ratio of the two responses

$$P_s(f) = \Gamma^2 \cdot \left| \frac{R_1(f)}{R_2(f)} \right|^2 \,. \tag{3.3}$$

The experimental BSC is proportional to this power spectrum, and has been derived for weakly-focused transducers [24], [25]. These proportionality factors are due to the diffraction effects from the transducer and the length of the gated region from the backscattered response used to estimate the power spectrum. The equation that was developed to estimate experimental BSCs is

$$\sigma_{BSC-\exp} = 2.17 \frac{z_0^2}{A_0 L} P_s(f) A_\alpha . \quad (3.4)$$

In this development, z_0 is the distance from the transducer to the scattering volume, A_0 is the area of the transducer surface, L is the axial length of the gated signal, and A_α is an attenuation correction factor.

3.2.2 Attenuation compensation

Because of the large impedance mismatch between the UCAs (specific acoustic impedance, Z_0 = 880 Rayl, for octafluoropropane in Definity UCAs) and the surrounding medium (water at 20° C, Z_0 = 1.5 MRayl), attenuation through a cloud of UCAs contributes heavily to the backscattered signal that is received. As a result, the signal power that is received by the ultrasonic transducer is reduced, which causes a reduction in the estimated concentration of UCAs. The attenuation is accounted for in the estimation of the BSC through an attenuation correction factor. Estimation of the attenuation correction factor has been approximated [48], and a more general correction factor that is valid for high number densities of evenly distributed scatterers has recently been derived [49]:

$$A_\alpha = e^{4\alpha_0(f)x_0} \frac{4\alpha^2(f)L^2}{\left(1-e^{-2\alpha(f)L}\right)^2} . \quad (3.5)$$

Here, $\alpha_0(f)$, $\alpha(f)$ are the attenuation coefficients (Np/cm) of the intervening medium before the gated region and the scattering medium within the gated region, respectively, and x_0 is the distance from the source to the gated region.

Because the medium was assumed to be a homogeneous mixture of UCAs and either degassed water or blood, the two attenuation coefficients, $\alpha_0(f)$ and $\alpha(f)$, were the

same. They were estimated during each trial using an insertion loss technique. The backscattered responses from a planar reference were collected before and after the UCAs were added. Their ratio is used to estimate the attenuation coefficient of the UCA cloud as follows:

$$\alpha = \alpha_{ref} + \frac{\ln(\zeta)}{4x_p} . \tag{3.6}$$

In this development, α_{ref} is the (known) attenuation coefficient of the medium without UCAs, ζ is the ratio of the frequency-dependent response without UCAs to the response with UCAs, and x_p is the total distance that the pulse must propagate through the cloud of UCAs in one direction.

3.3 Materials

3.3.1 Glass beads

Glass beads (Potters Industries Inc., USA) were used to validate the flow system experiments and the experimental estimation method of the BSC. Because the beads are manufactured with a distribution of sizes, it was necessary to sieve them before use in order to effectively compare the ESD estimates to the optically estimated diameters. Although it was desired to obtain glass beads with diameters comparable to UCAs (2-10 μm), the available equipment limited the smallest size beads that could be extracted to approximately 50 μm. After sieving, the beads were separated by mass according to the desired concentration for experiments, and then they were mixed with the appropriate amount of degassed water.

The sizes of the beads were estimated optically with a fluorescence microscope and camera system (Zeiss Axiovert 200M w/10x objective, Zeiss AxioCam MRm, Carl Zeiss Inc., Thornwood, NY) in standard bright field imaging mode. Images were captured with a resolution of 0.63 µm/pixel, based upon the magnification settings of the microscope. An example image of the glass beads under the microscope is shown in Figure 3.1.

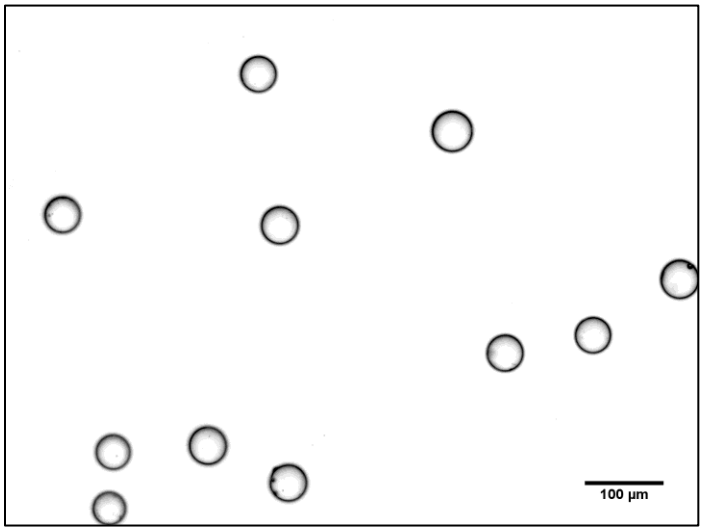

Figure 3.1 Bright field image of glass beads at a magnification of 10x

After capturing the images, a circular detection algorithm, developed by King and O'Brien [50], which utilizes the Hough transform, was used to obtain glass bead diameter estimates. The average size distribution is shown in Figure 3.2. The average bead diameter was 49.5 µm with a standard deviation of 2.76 µm.

3.3.2 UCAs

Definity UCAs, which have been approved for clinical use in the United States, were used in all of the experiments with UCAs. As reported by the manufacturer, Definity UCAs have a mean diameter of 1.1 – 3.3 µm, and 98% have a diameter smaller than 10 µm. Each vial contains 6.52 mg/mL of octafluoropropane and 0.75 mg lipid

blend in a sodium chloride suspension that is activated using the Vialmix sequence. This system agitates the Definity vial for 45 seconds for normal activation, and afterwards each mL of the solution is reported to contain at most $1.2x10^{10}$ microspheres.

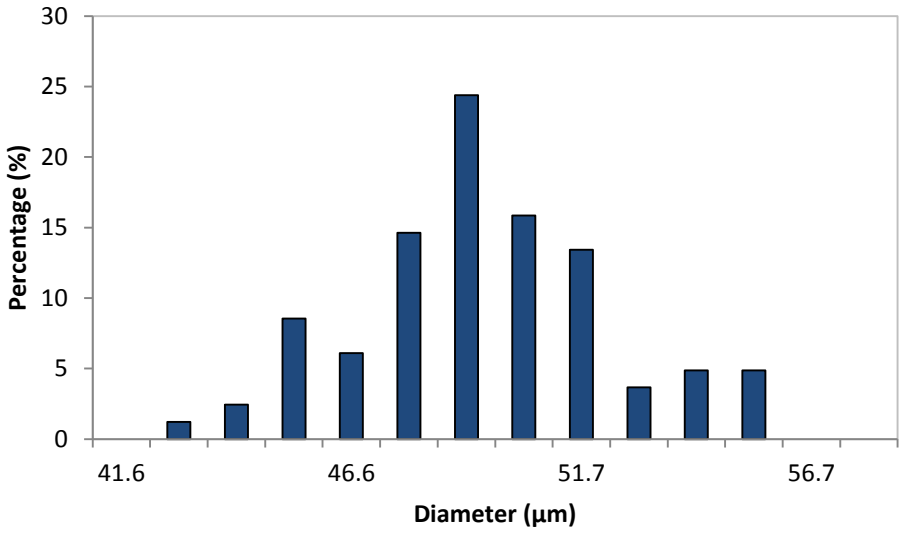

Figure 3.2 Estimated size distribution of glass beads

A similar procedure used to obtain size distribution estimates for the glass beads was used to estimate the sizes of the UCAs. Upon capturing bright field images of a sample of UCAs at a magnification of 63x (0.1 µm/pixel), the circular detection algorithm was applied. One of these gray scale images is presented in Figure 3.3. Resulting histograms were divided into 0.2-µm bins because this was the estimated uncertainty in the measurement. It was very important to obtain accurate estimates of size distributions because the resonance frequency of the bubbles is highly dependent upon shell parameters and UCA diameter [32]. Because different vials were used for separate trials of the experiments, variations in UCA size distribution among vials were considered. However, a single histogram of UCA size for many different vials was

created, and the mean diameter, standard deviation, and shape of the single histogram were similar to the histograms of the individual vials. Therefore, the single, large size distribution was used as a good estimate of the UCA sizes in the experiments, and this distribution is presented in Figure 3.4. The mean UCA diameter was 2.2 µm and the standard deviation was 0.71 µm, which is within the range of sizes reported by the manufacturer.

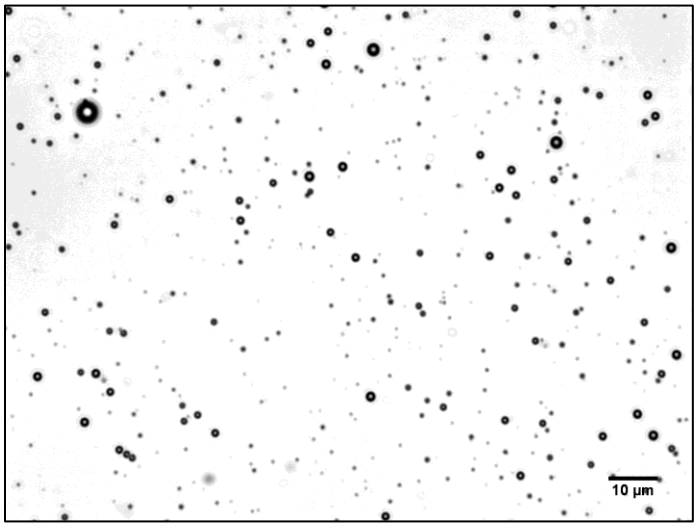

Figure 3.3 Bright field image of UCAs at magnification of 63x

Also, it is important to note that the UCAs can shrink over time. Dayton et al. [51] optically showed the gradual diffusion of gas from phospholipid- and albumin-shelled UCAs; some of the UCAs dissolved completely within minutes in their *in vitro* experiments. Droste [19] corroborated this effect in the body, reporting that the UCAs began to shrink within minutes of infusion. Because the BSC of UCAs depends significantly upon UCA size, it was necessary to consider the size distribution as a variable when estimating UCA concentrations from BSCs. In order to simplify complexity of the BSC calculation and enable faster UCA concentration estimates, a Gaussian size distribution was assumed for theoretical BSC calculations.

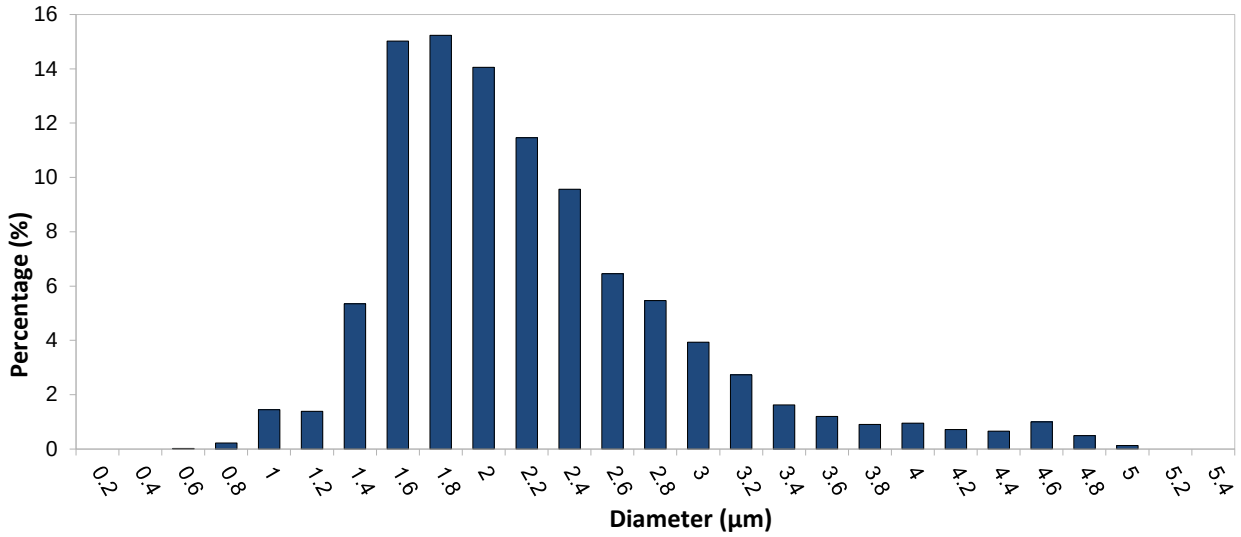

Figure 3.4 Estimated size distribution of UCAs

Other more complicated size distributions that more closely matched visually with Figure 3.4 were examined. Although these affected the shape of the theoretical BSCs at 1-14 MHz, UCA concentration estimates were not significantly affected because estimates were obtained using a frequency range above 14 MHz.

3.3.3 Experimental equipment

A transducer with a center frequency of 20 MHz, radius of 1/4 inch, focal distance of 3/4 inch (F-number of 3), and -10 dB bandwidth of 15-28 MHz was used to obtain all ultrasonic data. A pulser-receiver (Panametrics 5900, Waltham, MA), operating in pulse-echo mode with a pulse repetition rate of 1 kHz and a 26 dB gain, was connected to the transducer. Estimation of the PRP amplitude at the transducer focus for multiple input energies was accomplished using a membrane hydrophone (National Physics Laboratory, Teddington Middlesex, UK). Because the pulse was directed through an acoustically transparent well plate seal in all of the experiments, the hydrophone was placed behind one of these seals at the focus of the transducer during PRP amplitude

estimation. For input energies of 1, 2, 4, 8, and 16 μJ, the corresponding estimates of PRP amplitude were 70, 140, 270, 390, and 510 kPa. During all of the experiments, these settings were used in order to study the effects of PRP amplitude on UCA response.

The linear scattering model used to estimate UCA concentrations based upon experimental BSCs is only valid for small oscillations, and not for the large expansions associated with UCA collapse. Previous studies have estimated pressure amplitudes for Definity above which collapse begins to occur [52], [53]. Because this threshold is based upon the excitation frequency, PRP amplitude, length of the pulse, and size of the UCAs, it is difficult to use the previous data as an indication of whether collapse is occurring. In the previous studies mentioned above, the frequency was below 3 MHz, and the pressure threshold for 5% collapse varied from 600 kPa to 1.7 MPa. Therefore, collapse was minimized during the experiments presented in this work by using PRP amplitudes below 600 kPa and an excitation frequency range far above the resonance frequency range.

3.4 Methods

3.4.1 Hemacytometer based concentration estimates

After ultrasonic backscatter data was captured, a sample of the UCA and degassed water mixture was extracted from the apparatus being used in order to obtain hemacytometer based UCA concentration estimates for comparison to ultrasonic based estimates. This was performed for two of the experiments: the beaker experiments with UCAs in degassed water and the flow system experiments in degassed water. The

sample was extracted via a 1 mL syringe and an 18 gauge hypodermic needle in order to minimize the loss of UCAs through the opening of the syringe.

For each concentration estimate, a small amount of the extracted mixture was inserted into the 1/25 x 1/25 x 1/10 mm^3 hemacytometer (Bright-Line, Hausser Scientific, Buffalo, NY) chamber, which was divided into 25 laser-etched sections of equal volume. The number of UCAs in ten of the 25 sections was recorded, and the resulting concentration was converted to the number of UCAs per mL. Because the UCAs were much smaller than the hemacytometer chamber, they could easily move around while being counted. Often, the UCAs were not evenly distributed, and they moved due to their buoyancy and small currents in the chamber. For this reason, the hemacytometer based estimates were repeated six times for each experimental trial in order to estimate the average concentration of UCAs in the extracted mixture.

3.4.2 Beaker experiments

Initially, backscatter measurements were acquired with a beaker apparatus, modified to allow for the insertion and extraction of UCAs without moving any system components. A diagram and photograph of the chamber is shown in Figure 3.5. The chamber was first sealed with waterproof epoxy, and then two holes were drilled into the top. The first hole was sealed with an acoustically transparent well plate seal (Thermo-Scientific ABgene Adhesive Plate Seals, AB-0580, Hudson, NH) and the second was used for the insertion and extraction of degassed water and Definity UCAs. Backscatter data was acquired from the vertically mounted 20-MHz transducer, positioned above the seal so that the ultrasonic pulse was directed downward and normal to the seal. Within two centimeters below the seal, a flat Plexiglas reflector was fixed to allow for new

reference measurements to be taken with each trial. Because the reference measurements were acquired through the well plate seal, the transmission effects from the seal were included in the reference. A stir bar inside the apparatus was used to ensure an even distribution of microbubbles at the measuring site, and the entire chamber was placed in a tank filled with degassed water.

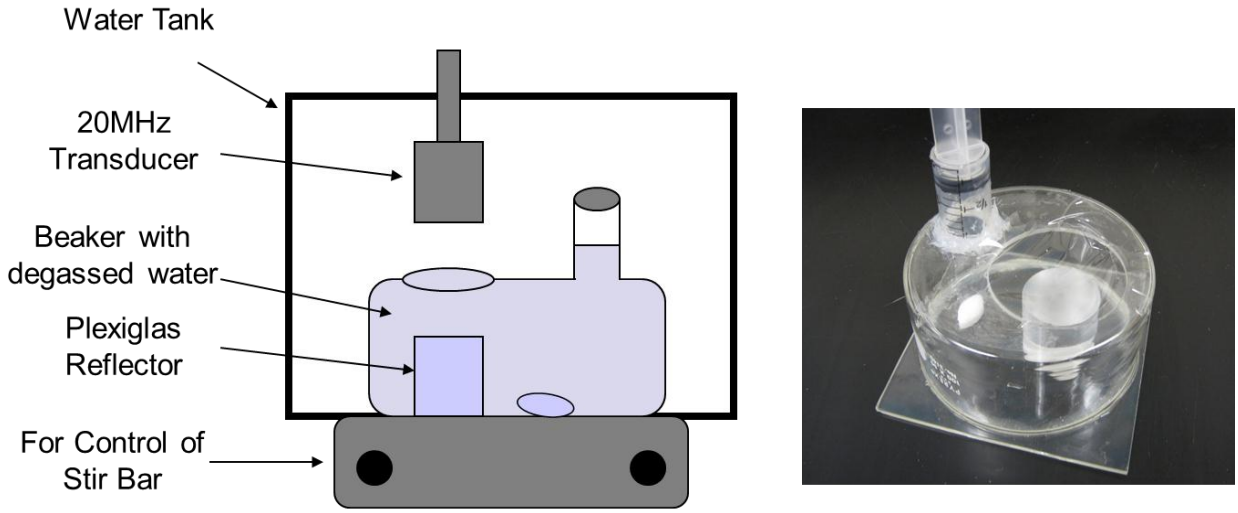

Figure 3.5 Experimental setup for the beaker system

After both reference measurements and noise floor estimates were recorded, the UCAs were inserted into degassed water with concentrations of 1x and 2x the dosage recommended by the manufacturer for diagnostic imaging, equal to $8x10^{-5}$ mL of Definity solution per mL. For each trial, 500 snapshots of the backscatter from the UCAs were acquired at three separate depths in the chamber. This was performed so that the distance between estimates was 4 mm. The transducer was then moved to place the focus back on the Plexiglas reflector so that reference measurements with the UCAs could be acquired. These were then used to estimate attenuation for each trial. Before the experimental BSC was calculated, the noise spectrum was subtracted. Also, the

axial length of the scattering volume used to calculate the normalized spectrum was equal to 15 times the wavelength of the 20-MHz pulse.

3.4.3 Flow system experiments

3.4.3.1 Description of the flow system and experimental procedure

The flow system was developed to emulate dynamic conditions like blood flow in the body. Powered by a peristaltic pump (Masterflex Variable Speed Economy Console Drive, Vernon Hills, IL), the system drew the UCA or glass bead mixture from a beaker to a specially designed Plexiglas® chamber. The chamber was built to increase the cross-sectional area of the flow from that of the tubing while minimizing sidewall effects and turbulence development near the measurement site. A diagram of the flow system and a photograph of the chamber are shown in Figure 3.6. After the mixture was drawn through the 3/8 inch opening at the bottom of the chamber, it rose vertically through the diverging opening, passing the measurement site when the cross section of the flow was 3/2 x 3/8 square inches. Two holes were drilled horizontally into the chamber: the lower hole was drilled at the measurement site, where one of the acoustically transparent well plate seals prevented the UCA mixture from escaping, and the upper hole contained a rubber stopper, from which a sample of the mixture could be extracted after the backscatter data was acquired. The 20-MHz transducer was positioned so that the ultrasound pulse was directed horizontally through the well plate seal and focused inside the chamber or at the back plane wall for reference measurements. After passing the second hole, the flow diverged again through the top 3/8 inch opening. Finally, the flow passed through the pump and was discarded into the original beaker, where a large stir bar kept the mixture from separating.

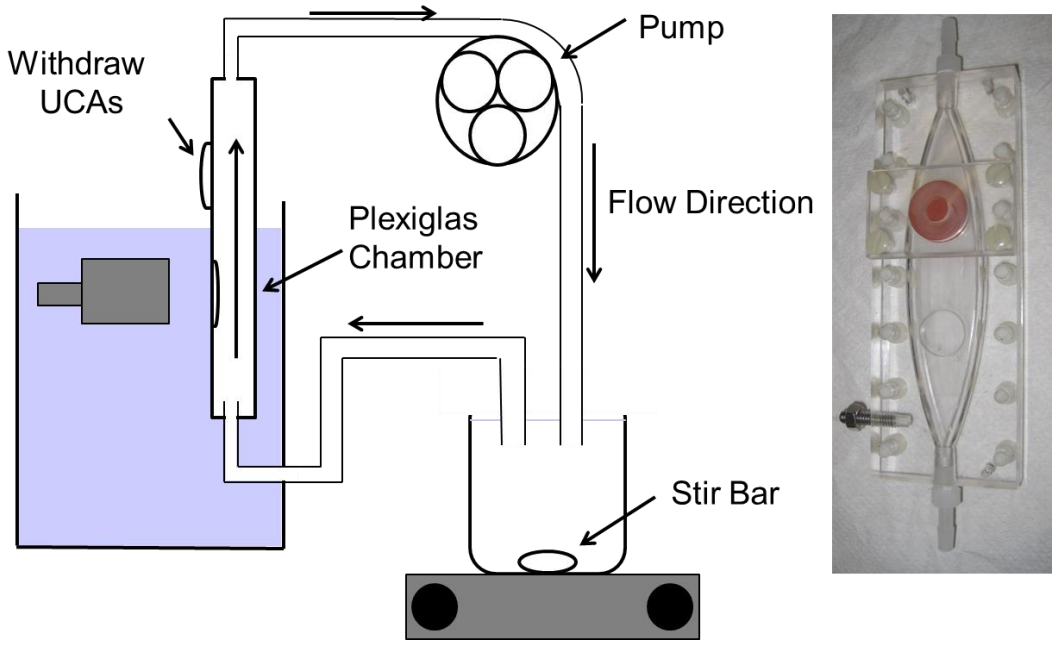

Figure 3.6 Diagram of the flow system indicating location of the flow chamber, transducer, and pump, and corresponding photograph of the chamber

In order to estimate the BSC, estimates of the pulse-echo impulse response of the transducer were approximated by capturing the reflections from the pulse focused at the back plane wall of the Plexiglas chamber when only degassed water flowed through the system. These reference measurements were used to eliminate the system dependent characteristics, as detailed in Section 3.2.1. An estimate of the noise floor spectrum was also obtained by focusing the pulse inside the chamber filled with water. After inserting UCAs or glass beads, 500 or 1000 snapshots of the backscattered ultrasound from the mixture were procured. Reference measurements of the back plane wall were repeated in order to estimate attenuation for each trial. The backscattered snapshots were gated around the location of the focus, such that the length of the gate was equal to 15 times the wavelength of the 20-MHz pulse. Before calculating the normalized power spectrum, the noise spectrum was subtracted.

3.4.3.2 Experiments with glass beads in degassed water

Initial experiments with the flow system were conducted with glass beads in degassed water. Concentrations of 5 g and 10 g of beads in 500 mL of degassed water were inserted into the beaker before backscatter estimates were obtained. Because the upward flow inside the chamber worked against the natural tendency of the beads to settle downward, the flow rate was adjusted to 1320 mL/min during all trials. Also, the speed of the stir bar in the beaker was increased to prevent settling inside the beaker. This speed was adjusted until the cloud of beads was visibly distributed throughout the beaker.

Because the average diameter of the beads was estimated with a microscope to be 49.5 μm, the concentrations used in each trial were too low to use the hemacytometer for verification. This is because as the diameter of an object increases, fewer of those objects are required to obtain the same concentration value. Because the concentration of glass beads inside the chamber might not have been the same as the concentration of beads inserted into the beaker, a more accurate technique for verifying the concentration inside the chamber was developed. After measurements of the backscatter from the beads were acquired, 100 mL of the bead and degassed water mixture that exited the chamber was collected. The mixture was then heated to separate the glass beads from the water, and the final mass of beads was used to determine the overall concentration.

3.4.3.3 Experiments with UCAs in degassed water

After experiments with glass beads in degassed water were conducted, trials with UCAs in degassed water were performed. For these experiments, concentrations of 1x,

2x, and 5x the concentration recommended by the manufacturer for imaging ($8x10^{-5}$ mL of Definity solution per mL) were used. The physical properties of the UCAs are different from the glass spheres, and so procedures were adjusted as follows. Because the UCAs flowed vertically upward, they moved in the direction of the natural buoyant force that acted upon them. Also, UCAs are easily destroyed when subject to stresses such as high flow rates, overly rigorous mixing, and the mechanical motion of the pump, which will reduce the number of UCAs in the system. Therefore, the flow rate was reduced to approximately 350 mL/min.

In order to estimate the available timeframe for acquiring estimates before the loss of UCAs in the system significantly reduced the ultrasonically estimated UCA concentration, an additional trial was performed. After insertion of a 1x concentration of UCAs, 1000 snapshots of the backscatter were acquired every 5 minutes over a period of 15 minutes. After 10 minutes, the estimated concentration of UCAs was reduced by approximately 2%, and after 15 minutes, the estimated concentration had decreased by just less than 5%. All of the ultrasonic data from the regular trials was acquired within 7 minutes after the UCAs had been inserted into the beaker, and so the estimates of concentration were minimally affected by the rate of UCA loss in the system.

3.4.3.4 Experiments with UCAs in blood

The final experimental trials were performed with UCAs in porcine whole blood. Immediately after fresh porcine blood was collected, 3 g/L of ethylene diamine tetra acetic acid (EDTA) was added and thoroughly mixed to prevent coagulation. The amount of anticoagulant used was based upon the concentration of EDTA used in previous studies with whole blood [46], [54]. Care was taken to ensure that the blood

was constantly mixed, and all experiments were performed within six hours of the blood acquisition in order to ensure freshness.

The BSC of blood was used as a reference in order to estimate the BSC of UCAs in blood. The reason for this choice is because, in order to account for all system dependencies and attenuation at the site of interrogation *in vivo*, a reference at that site is required. The ratio of the backscattered power from blood with UCAs to blood alone can be represented as follows, assuming that the scattering from blood and UCAs together is the sum in the time domain of the scattering from blood and UCAs alone:

$$\frac{\left|R_{(UCA+b)}(f)\right|^2}{\left|R_b(f)\right|^2} = \frac{\left|S_{UCA}(f)\right|^2}{\left|S_b(f)\right|^2} + 1 + \frac{S_{UCA}(f)}{S_b(f)} + \frac{S_{UCA}^*(f)}{S_b^*(f)}, \tag{3.7}$$

where $|R_{UCA+b}(f)|^2$ is the backscattered power spectrum from the UCAs in blood, $|R_b(f)|^2$ is the backscattered power spectrum from the blood alone, S_{UCA} and S_b are the magnitudes of the backscattered response in the frequency domain, and the * corresponds to the complex conjugate of the response. If the ratio of S_{UCA} to S_b is much greater than one, then only the squared term on the right-hand side dominates. Therefore, the power spectrum of the UCAs, $|S_{UCA}(f)|^2$, can be estimated if $|S_b(f)|^2$ is known.

Using the development from Chapter 2.4 for calculating $\sigma_{BSC\text{-}blood}$, the estimated BSC of UCAs in blood is

$$\sigma_{BSC-UCAs} = \sigma_{BSC-blood} \cdot \frac{\left|R_{(UCA+b)}(f)\right|^2}{\left|R_b(f)\right|^2}, \tag{3.8}$$

where $\sigma_{BSC\text{-}blood}$ is the BSC of blood alone. Therefore, in order to estimate the BSC of UCAs in blood, it is necessary to acquire the backscattered response from the blood

alone. The BSC of blood alone was estimated for comparison to theoretical calculations of blood BSC. To do this, the same procedure, as outlined in Section 3.4.3.1 and including the subtraction of the noise floor and the same length of the gated window, was used to estimate the normalized power spectrum. First, reference measurements of the back planar wall of the flow system chamber were acquired with only degassed water in the system. Next, the focus of the transducer was positioned inside the chamber to obtain an estimate of the noise floor spectrum. After insertion of the blood into the system, 500 or 1000 snapshots of the backscatter were used to obtain estimates of blood BSC, and the reference measurements were repeated with the blood inserted to estimate the attenuation through blood for each trial.

After estimates of the backscattered power from blood were acquired, the UCAs were inserted into the beaker at a concentration of 2x the dosage recommended by the manufacturer. Backscatter data was captured for the UCAs in blood, as well as a reference measurement for attenuation estimation.

3.4.4 UCA concentration estimation

Ultrasonic based UCA concentration estimates were obtained by fitting the experimental BSC to the linear theoretical scattering model reviewed in Section 2.3.1To perform the fitting, a Levenberg-Marquardt algorithm [55], [56] was implemented in Matlab (MathWorks, Natick, MA). This recursive method for nonlinear least squares minimization combines the method of gradient descent with Gauss-Newton iteration and was implemented using three variables. Assuming fixed shell parameter S_p, shell friction S_f, and surface tension τ, with values provided in Table 2.1, the UCA size distribution parameters and the UCA concentration define the theoretical linear BSC of UCAs for a

fixed frequency range. As explained in Section 3.3.2, a Gaussian size distribution was used to simplify computation; therefore, the two other variables in the estimation technique were the size distribution parameters: mean diameter and standard deviation in diameter of the UCAs. The procedure for fitting each experimental BSC to a theoretical one was as follows: first, initial guesses for the three variables were used to calculate a theoretical BSC. Next, the root mean square error (RMSE) was calculated between the theoretical and experimental BSCs. Using the Levenberg-Marquardt formulation, a new theoretical BSC was derived, the RMSE was recalculated, and it was compared to the previous RMSE value. The algorithm was programmed to stop when 10,000 iterations were reached or the RMSE did not improve by more than 0.1% from the previous iteration. The outputs of the algorithm included the final estimated concentration of UCAs, mean UCA diameter and standard deviation, number of iterations, and total time required for convergence. Matrix operations were used in the Levenberg-Marquardt formulation, and so if one of these matrices became singular during the iterative process, the algorithm would return an error. In this case, the algorithm did not converge to an estimate of UCA concentration.

Because initial guesses for the three variables were required to begin the estimation sequence, the final concentration estimate may have been sensitive to these guesses. However, the regions of convergence for the algorithm were not rigorously determined in this work. Instead, a more simplified procedure was used to examine the effects of initial guesses on the UCA concentration estimate, and this procedure is outlined here. For each trial, regardless of the concentration of UCAs that was inserted into the beaker, the initial guess for UCA concentration was first set to 9.6×10^5

UCAs/mL, which corresponds to the 1x dosage recommended by the manufacturer. The initial size distribution parameters were fixed at 2.2 μm for the mean diameter and 0.71 μm for the standard deviation because these were the parameters from the optical estimate of UCA size distribution. Next, the initial UCA concentration was varied to find a range of initial guesses for concentration that led to convergence of the algorithm. It was found that for all trials, the algorithm converged only for initial concentrations within 100 times the final estimate, and that it converged to the same concentration estimate for all initial values of concentration within that range. This was the final concentration estimate that was reported in the results.

The limits for initial guesses of the size distribution parameters were also interrogated. The initial UCA concentration value was fixed to within 100 times the final concentration estimate, and the initial values for mean diameter and standard deviation were varied. The limits of the initial values were 1 to 8 μm and 0.4 to 3 μm for the mean diameter and standard deviation, respectively. These limits were based upon the limits of the UCA size distribution estimates and the size limits reported by the UCA manufacturer. When the initial size distribution parameters were varied within these limits, the resulting UCA concentration estimates differed by less than 2% for all trials. Therefore, it was concluded that the initial values of the size distribution parameters were not a limiting factor for the UCA concentration estimates reported in this work.

3.5 Simulations of the BSC

A simulation was developed in Matlab to estimate the BSC based upon the nonlinear model for UCA dynamics presented in Section 2.3.2. The model is used to estimate the oscillatory behavior of UCAs exposed to an ultrasound pulse, which

produces a pressure wave that propagates back to the insonifying transducer. The pressure waves from each UCA in the insonified volume are summed at the insonifying transducer surface to simulate the received response. An overview of the simulation is presented here.

The simulation requires inputs of size distribution parameters and the PRP amplitude of the insonifying pulse. First, the scattering volume was defined as a rectangular prism, where two sides had equal lengths of twice the wavelength of a 20 MHz transducer times the F-number, and the third side had a length of 15 times the 20 MHz wavelength. The total volume was 0.60 mm^3. The volume was discretized both uniformly and so that the minimum distance between any two points in the volume was 10 μm. Based upon the input value for the concentration of UCAs and the total volume, the number of UCAs inside the scattering volume was determined.

In order to simulate the average response rather than an individual one, the simulation was repeated 500 times for each BSC estimate. For each of the responses, new locations for all of the UCAs inside the scattering volume were randomly assigned. Each UCA in the volume was also assigned a resting diameter based upon the input size distribution parameters. Next, a 20-MHz center frequency Gaussian pulse with a fractional bandwidth of 80% was generated to imitate the impulse response of the transducer used in the experiments. Field II [57], [58], a program developed to simulate the spatial impulse response of a transducer with finite dimensions as a sum of discrete point sources, was used to estimate the spatial impulse response for a concave circular transducer with the same dimensions and focal length as the 20 MHz transducer used in the experiments. The time-varying pressure at the location of each UCA in the field of

the transducer was calculated as the convolution of the spatial impulse response with the generated Gaussian impulse response of the transducer [57]. After the input pressure for each UCA was normalized to the desired PRP amplitude, the equation of motion presented in Equation 2.8 was used to estimate radius versus time curves based upon each calculated input pressure.

Assuming that each UCA acted as a spherical source, the far field pressure wave front was spherically shaped. In the simulation, the ultrasonic response obtained by the transducer was assumed to be due to UCA oscillations and not due to scattered reflections of the pulse. This assumption was based upon a previous study [59] that reported that the error due to neglecting the passive part of scattering from UCAs was less than 0.25% for $R_0 < \lambda\sqrt{3}/2\pi$, where λ is the wavelength of the applied ultrasound. At 28 MHz, approximately the smallest wavelength used to excite the UCAs in the simulation, this limiting radius is about 15 μm, which is much larger than the radii of Definity UCAs. Neglecting any multiple scattering effects, the simulated response obtained by the transducer was estimated as the sum of the scattered pressures from each UCA, shifted in time according to their distances from the transducer surface. This time shift was calculated by convolving the scattered pressures with their corresponding spatial impulse responses and the Gaussian impulse response of the transducer.

After the simulation acquired 500 responses for each set of randomly distributed UCAs, the simulated reference response was generated using the reflection coefficient of a Plexiglas plate. Finally, Equation 3.4 was utilized to estimate the BSC using the nonlinear model. The results for the estimated BSCs of UCAs from this simulation were then compared with experimental BSC estimates and theoretical calculations with the

linear model. Figure 3.7 presents a diagram of the simulation with the major steps highlighted.

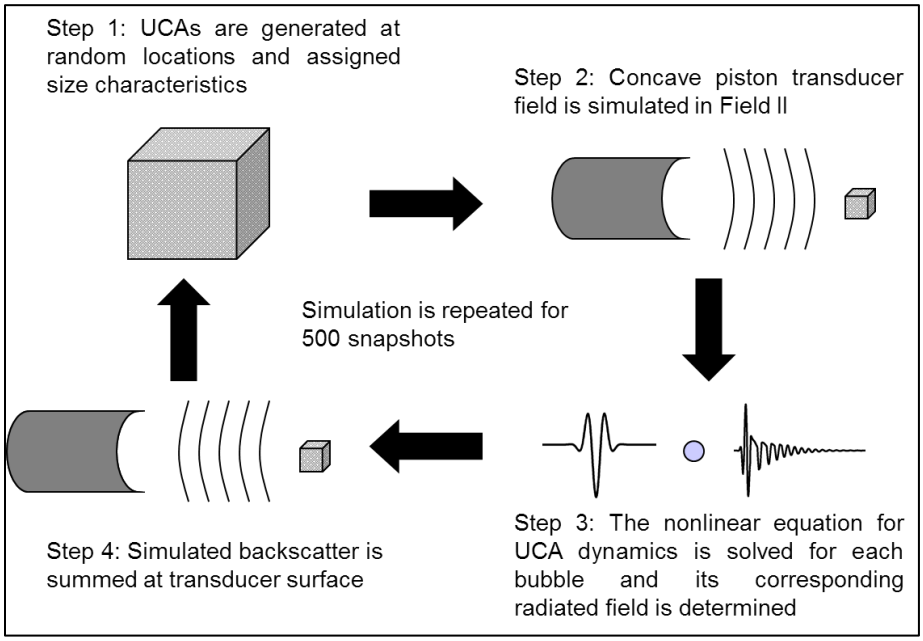

Figure 3.7 Overview of the simulation steps used to estimate the BSC of UCAs with the nonlinear model for UCA dynamics

CHAPTER 4 RESULTS

4.1 Theoretical BSCs of UCAs

The linear model was used to estimate the BSC for varying parameters of the Gaussian UCA size distribution in order to determine an optimal frequency range for extracting UCA concentration estimates. Over the optimal range of frequencies, changes in the size distribution would have a minimal effect on the BSC, and therefore the concentration of UCAs would dominate. Using Equation 2.4, the scattering cross sections for single UCAs of varying radii were calculated. These were used to determine the relative contributions of UCA size, and whether the differences in the radii of a polydisperse scattering volume of UCAs would significantly affect the shape of the BSC. Figure 4.1 shows the scattering cross sections of UCAs with radii from 0.25 to 5 μm based upon the linear model.

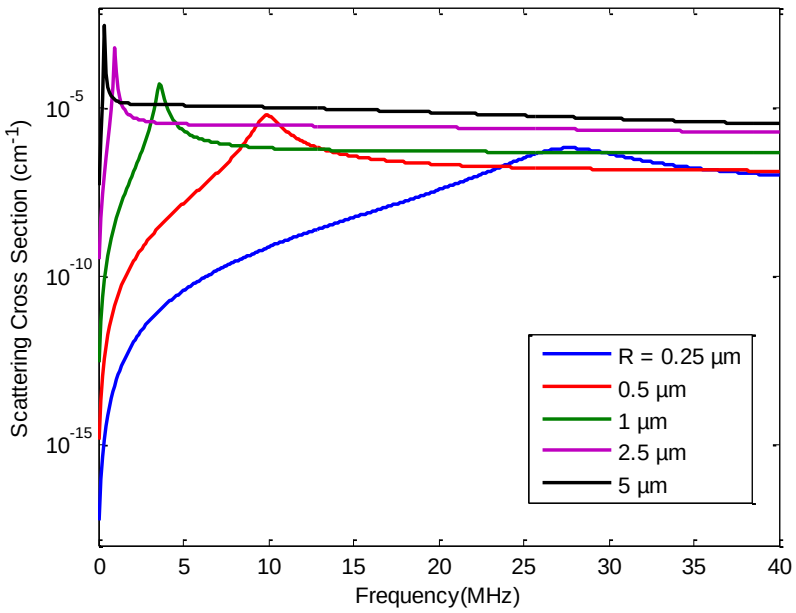

Figure 4.1 Scattering cross sections for single UCAs of various diameters, calculated using the linear model

Because the scattering cross sections of the larger UCAs dominated the contributions to the BSC and the estimated UCA size distribution contained a large number of UCAs with 0.4-1.5 μm radii, the contributions of the smaller UCAs with resonant frequencies close to 20 MHz were insignificant compared to the larger UCAs with resonant frequencies near 4-12 MHz. It was therefore determined that the optimal frequency range for extracting UCA concentration estimates was above 4-12 MHz. Above 12 MHz, the resonant frequencies of the UCAs could be avoided where nonlinear oscillations were more likely to occur. Although different UCA scattering models usually predict slightly different resonance frequencies, knowledge of the exact resonant frequency was not necessary when estimates were extracted from scattering behavior above 14 MHz.

The collective effects of a polydisperse scattering volume on the theoretical BSC were also examined. This was achieved by holding one of the size distribution parameters constant while varying the other. For a Gaussian size distribution with parameters of mean UCA diameter and standard deviation in diameter, this technique was used to calculate the theoretical BSC. In Figure 4.2, the mean UCA diameter was fixed at 2.2 μm and the standard deviation was varied from 0.3 to 1.5 μm. Figure 4.3 shows the BSC when the standard deviation was held constant at 0.71 μm and the mean UCA diameter was varied from 0.8 to 3.6 μm. The fixed parameters were obtained by fitting a Gaussian distribution to the optical size distribution estimate of the UCAs for all vials of Definity combined. The estimated size distribution in each individual vial was also fit to a Gaussian distribution. The ranges of size distribution parameters

that were examined were based upon the results from fitting the Gaussian distribution to the individual vials.

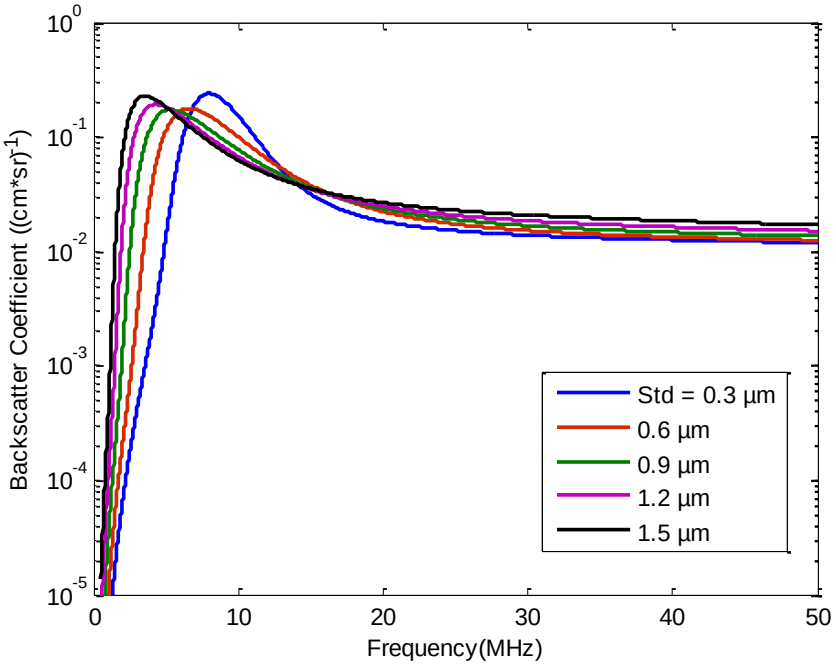

Figure 4.2 Theoretical BSC of UCAs calculated using the linear model, a Gaussian size distribution, and the following parameters: a constant mean UCA diameter of 2.2 µm and varying standard deviations in diameter

For the mean diameters less than 2.2 µm in Figure 4.3, the resonant peak was not nearly as steep. This can be explained based upon the results and short discussion of Figure 4.1. Although the smaller UCAs had resonant frequencies that should have shifted the peak toward higher frequencies, the contributions from the larger UCAs dominated, and the result was a broadening of the resonant peak. In order to determine the frequencies at which the changes in Gaussian size distribution parameters would have the least effect on the theoretical BSC of UCAs, the curves in Figure 4.2 and Figure 4.3 were compared as follows: the curve with the largest magnitude BSC was subtracted from the curve with the lowest magnitude, and the frequency at which this

difference was minimized corresponded to the least change in BSC due to changes in size distribution.

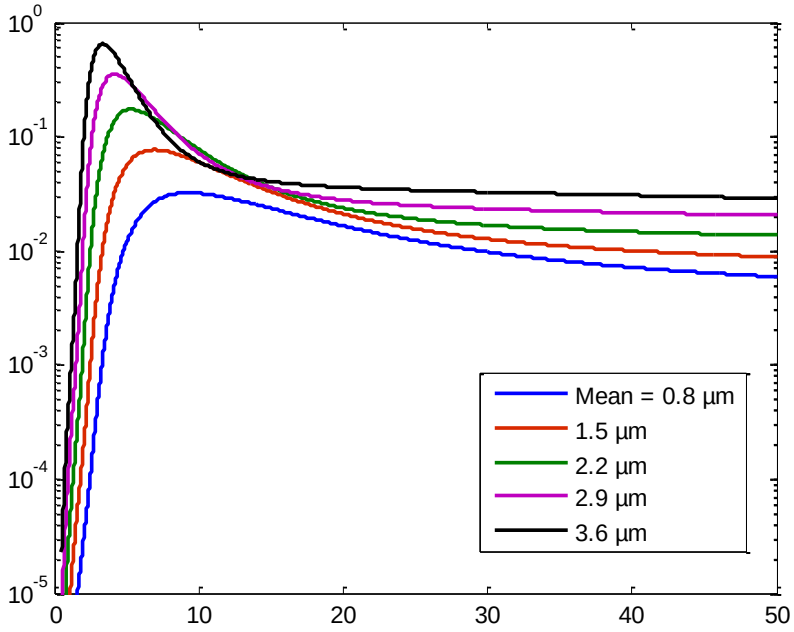

Figure 4.3 Theoretical BSC of UCAs calculated using the linear model, a Gaussian size distribution, and the following parameters: a constant standard deviation in UCA diameter of 0.71 µm and varying mean diameters

In Figure 4.2 this minimum difference occurred at 14 MHz, and the change in BSC remained approximately constant from 14 to 50 MHz. In Figure 4.3, the minimum difference between BSCs also occurred at 14 MHz, but the difference increased again from 14 to 50 MHz. From 14 to 30 MHz, the differences were smallest for both figures and the changes in mean diameter changed the slope of the BSC curve but did not affect its magnitude significantly. On the other hand, the greatest difference between BSCs in both figures occurred below 12 MHz because this was where the resonance of the larger UCAs dominated the scattered power.

Based upon this analysis, a 20 MHz transducer was chosen for the experiments because the corresponding -10 dB bandwidth was 15-28 MHz. Using this range to

extract estimates of UCA concentration ensured that the changes in standard deviation of UCA diameters would have a minimal effect on the BSC and that the changes in mean diameter would affect the BSC in a predictable way. This allowed the Levenberg-Marquardt regression to converge to a more robust UCA concentration estimate using less iteration. Because the experimental BSC was found to deviate from the linear model's predictions above 25 MHz, the frequency range used to extract concentration estimates was modified to 15-25 MHz, and this was the range used for all the UCA concentration estimates reported in this work.

4.2 Theoretical BSCs of blood

The parameters from the theoretical BSC of blood, calculated using Equation 2.11, were also varied to determine the effects of aggregate diameter and hematocrit on the theoretical BSC of blood. The hematocrit was varied from 30% to 55% to reflect the hematocrits of whole blood. Aggregate diameter, on the other hand, was varied from 0.2 to 1.0 RBCs per aggregate. Although an aggregate diameter of less than 1.0 RBCs does not correspond to a physical aggregate of RBCs, the previous experimental estimates of blood BSC have been fit to the theoretical approximation, and an aggregate diameter approximation of less than 1.0 RBCs was common for whole blood [46]. To examine the effects of each parameter on the calculation of the blood BSC, a technique similar to that described in Section 4.1 was used. First, the aggregate diameter was held constant at 0.5 RBCs, and the hematocrit was varied from 30% to 55%. The resulting BSCs are shown in Figure 4.4.

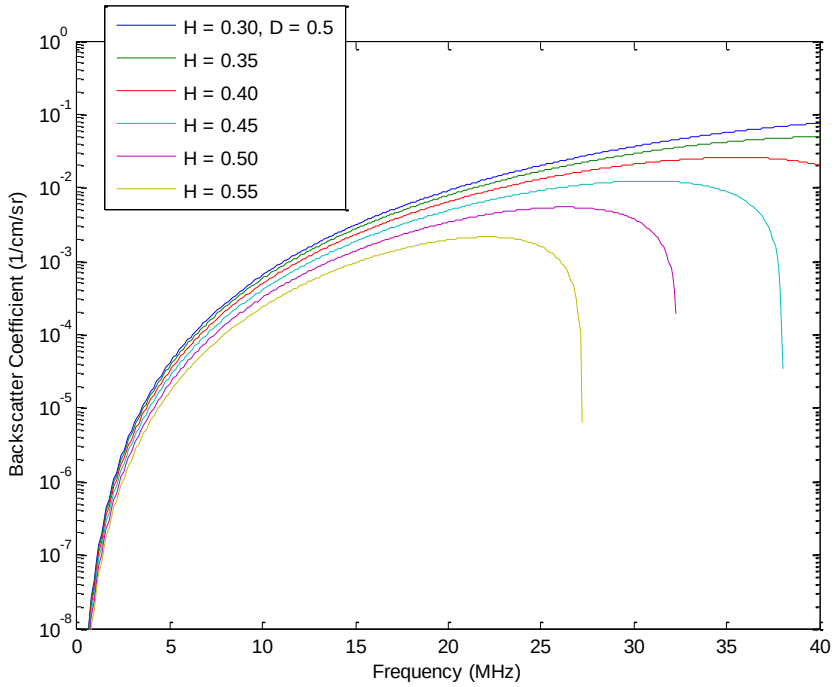

Figure 4.4 Theoretical BSC of blood for fixed aggregate diameter (D) in number of RBCs and varying hematocrit (H), which is reported as the volume fraction of RBCs in whole blood

As the hematocrit increased, the slope of the BSC decreased. Also, because the structure factor (SF) in Equation 2.12 was approximated to second order, its accuracy was limited to lower frequencies. The SF was approximated as the difference between the packing factor (the low frequency limit of the SF) and a frequency-dependent term that incorporated the aggregate diameter. When the packing factor was less than the aggregate diameter term, the approximation resulted in a negative BSC, which is not physically possible. Therefore, the limit of the SF approximation was based upon the frequency at which the BSC dropped rapidly and became negative. This frequency was called the cutoff frequency in this work. In Figure 4.4 the cutoff frequency decreased as hematocrit increased because the packing factor of flat disks was dependent upon the hematocrit.

Changes in BSC due to a varying aggregate diameter were also investigated. In Figure 4.5 the theoretical BSC of blood was calculated for a fixed hematocrit of 40% and an aggregate diameter that varied from 0.2-1.0 RBCs. As aggregate diameter increased, the slope of the BSC decreased. Also, the cutoff frequency was significantly reduced to approximately 23 MHz for an aggregate diameter of 1.0 RBCs. This was because the aggregate diameter term directly affected the SF approximation. Because the frequency range used in the experiments with blood was 15-25 MHz, the approximation for the SF had a large effect on the theoretical BSC of blood used as a reference to estimate the BSC of UCAs. For this reason, and to simplify the calculation, the aggregate diameter was set to zero for the initial experiments with UCAs in blood.

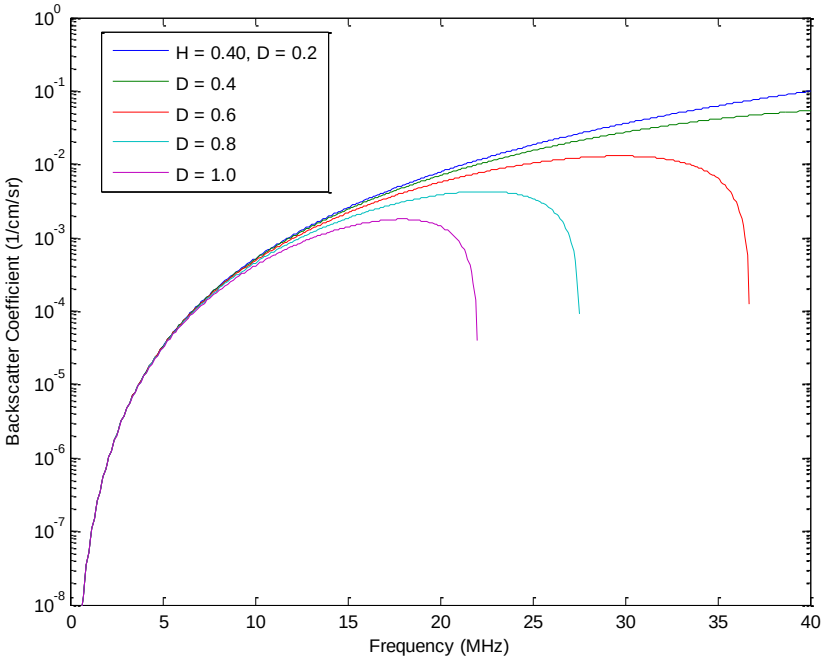

Figure 4.5 Theoretical BSC of blood for fixed hematocrit (H), which is reported as the volume fraction of RBCs in whole blood, and varying aggregate diameter (D) in number of RBCs

4.3 Experimental results from the beaker experiments

Results for the beaker experiments were collected for multiple trials and iterations to improve the estimation of the BSC and the hemacytometer based UCA concentration estimates. The estimated attenuation and BSCs from three different depths in the beaker, separated by 4 mm, are shown in Figure 4.6 and Figure 4.7 for the final trial. The peak of the attenuation coefficient is near 16 MHz and then it decreases to less than 5 dB/cm at about 25 MHz. Ultrasonic data was acquired after a 1x concentration of UCAs had been inserted and allowed to mix for one minute. The incident PRP amplitude used to obtain the BSCs in Figure 4.7 was 140 kPa.

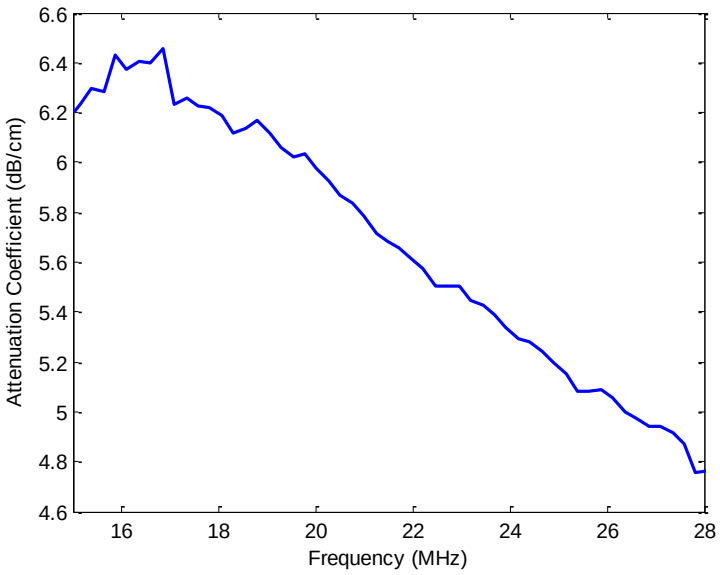

Figure 4.6 Attenuation coefficient of UCAs in the beaker experiments, where the UCAs were inserted at 1x concentration, and for a PRP amplitude of 140 kPa

UCA concentration estimates were obtained for the three estimates of BSC corresponding to locations inside the beaker. Hemacytometer based estimates were also acquired at two heights inside the beaker. The locations inside the beaker where the mixture was extracted were visually matched to the approximate location at which

the BSC was estimated. Because this was difficult to visually estimate, only two locations (top and bottom) were acquired. The results of the hemacytometer based estimates of UCA concentration, the corresponding ultrasonic based estimates, and the total time for the Levenberg-Marquardt regression to converge are reported in Table 4.1.

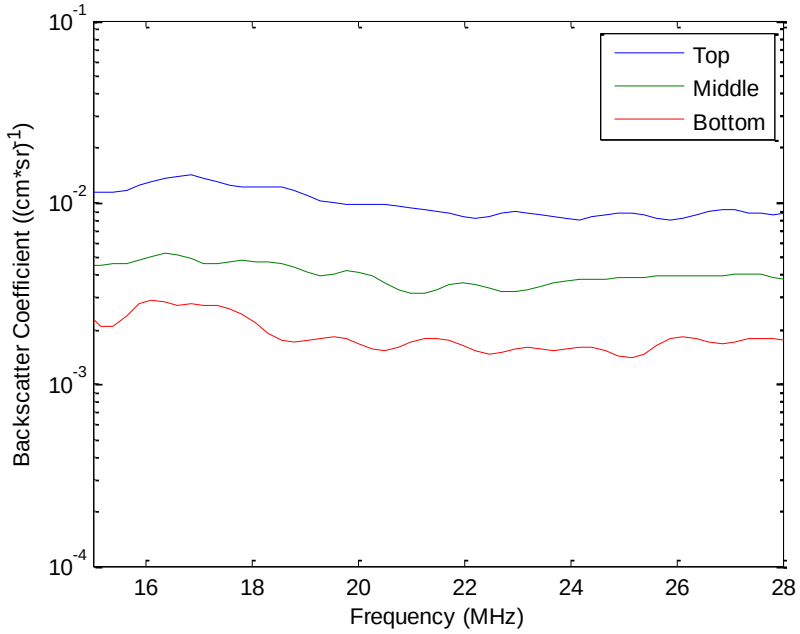

Figure 4.7 Estimated BSC of UCAs inserted at 1x concentration for various heights (top, middle, bottom) inside the beaker, each separated by 4 mm, and for an incident PRP amplitude of 140 kPa

Table 4.1 UCA concentration estimates at various heights inside the beaker, where each location is separated by 4 mm

Position in Beaker	top	middle	bottom
Hemacytometer Based Concentration (UCAs/mL)	3.8 ± 0.8E+06	N/A	3.0 ± 0.7E+05
Estimated Concentration (UCAs/mL)	4.9E+06	1.5E+06	8.5E+05
Elapsed Time to Converge (s)	0.26	0.13	0.14

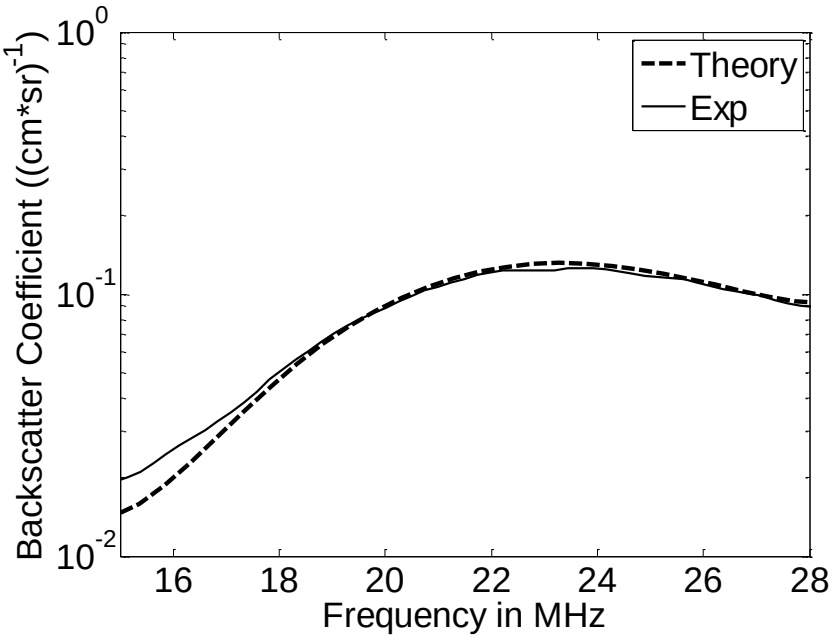

Figure 4.8 Estimated BSC and corresponding Faran theory for 5 g of glass beads in 500 mL of degassed water

4.4 Experimental results from the flow system

4.4.1 Glass beads in degassed water

The resulting BSCs and corresponding Faran theory for one trial of the two concentrations used with the glass beads is presented in Figure 4.8 and Figure 4.9. The frequencies presented in the figures were used for ESD and ESC analysis and were based upon the -10 dB bandwidth of the 20-MHz transducer. The estimates of these parameters are presented for the trials shown in the figures as well as for another trial in Table 4.2. The reported concentration was determined by heating the glass bead and UCA mixture and estimating the final mass of beads, as explained in Section 3.4.3.2 For both trials, ESD estimates were no more than 1.6% different from the optically estimated mean size of 49.5 μm. Also, for the first trial, the ESC was within 3.4% of the lower bead concentration estimate, acquired using the water evaporation technique,

and within 2.4% of the higher concentration estimate. For the second trial, the lower concentration estimate differed from the ESC by 6.4% and the higher concentration differed by 2.8%.

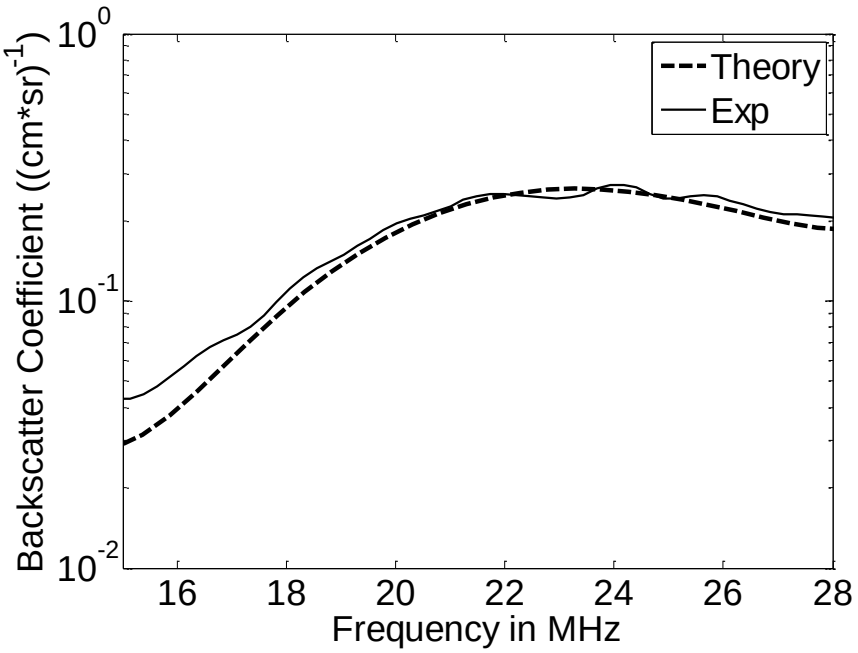

Figure 4.9 Estimated BSC and corresponding Faran theory for 10 g of glass beads in 500 mL of degassed water

Table 4.2 Estimated glass bead concentrations and diameters, using a water evaporation technique and an ultrasonic, BSC-based technique

Trial 1		
ESD (µm)	49.5	49.5
ESC (beads/mL)	4.8E+04	1.00E+05
Estimated Concentration (beads/mL)	5.0E+04	9.9E+04
Trial 2		
ESD (µm)	48.7	48.8
ESC (beads/mL)	4.7E+04	1.03E+05
Estimated Concentration (beads/mL)	4.4E+04	1.06E+05

4.4.2 UCAs in degassed water

Attenuation estimates were acquired for each trial with the UCAs in degassed water in order to more accurately compensate for attenuation in the system. Because the trials were performed for varying incident PRP amplitudes, the corresponding attenuation coefficient was used to estimate the BSCs. The estimated attenuation for varying PRP amplitude is shown in Figure 4.10 for one trial of each of the 1x, 2x and 5x concentrations used in the experiments. For all trials, the attenuation coefficient peaked somewhere below 15 MHz and decreased with increasing frequency. For lower frequencies, the attenuation increased with increasing PRP amplitude; however, above approximately 20 MHz, the attenuation was not significantly dependent upon PRP amplitude. This indicated that the incident PRP amplitude was important for estimating attenuation for excitation frequencies close to the resonant frequencies of the majority of the UCAs, but the PRP amplitude was less important for higher excitation frequencies.

The BSC results for varying incident PRP amplitude and a single trial for each of the concentrations is shown in Figure 4.11. The BSCs correlate well with the predictions of the linear model, as in Figure 4.2 and Figure 4.3. That is, for a poly-disperse volume of randomly distributed UCAs with estimated mean diameter of 2.2 μm, the BSC decreases and then stays relatively constant for increasing frequency. Also, for increasing PRP amplitude the BSCs are not the same as predicted by the linear model. This indicates that nonlinear UCA behavior is present even for incident PRP amplitudes as low as 390 kPa. The corresponding UCA concentration estimates decreased with increasing PRP amplitudes as is evident in the estimated BSCs (Figure 4.11).

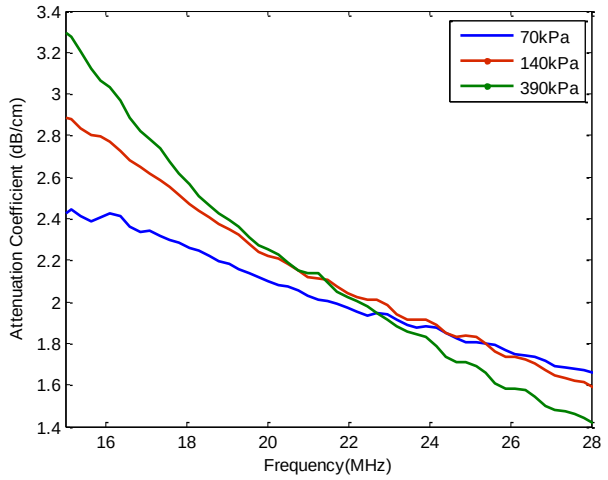

(a)

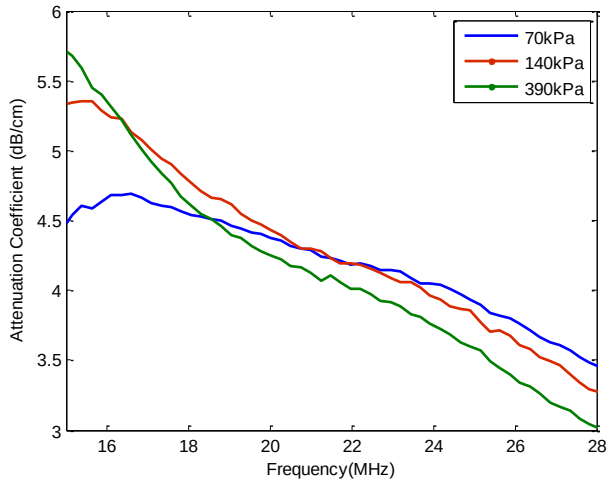

(b)

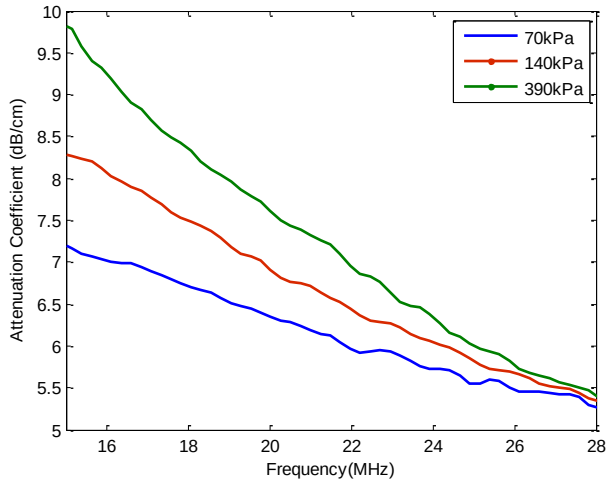

(c)

Figure 4.10 Attenuation coefficient of UCAs in degassed water versus frequency for varying incident PRP amplitudes (in kPa) and UCA concentrations of (a) 1x, (b) 2x, and (c) 5x dosage

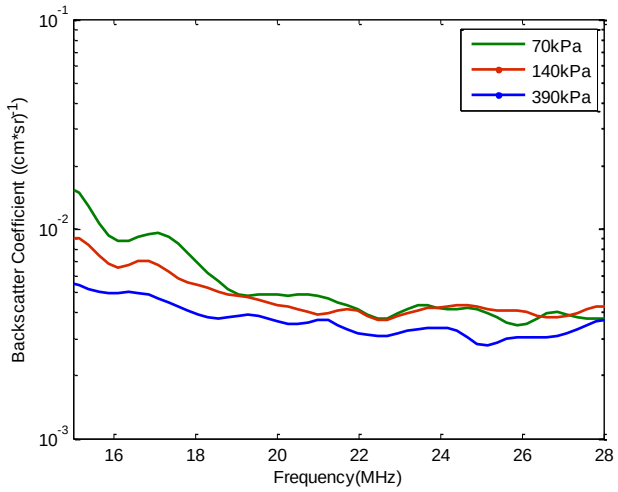

(a)

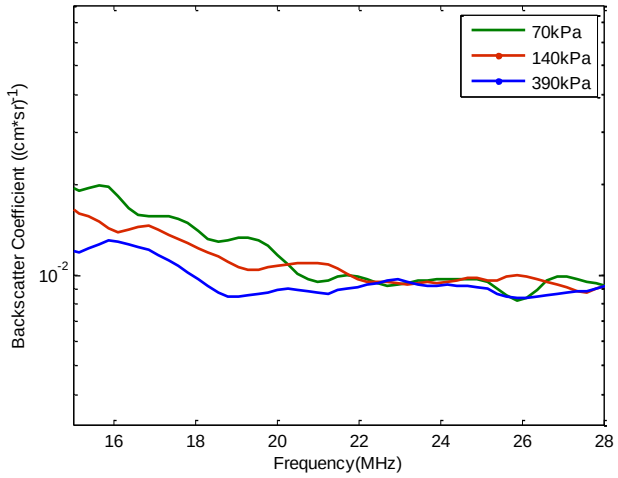

(b)

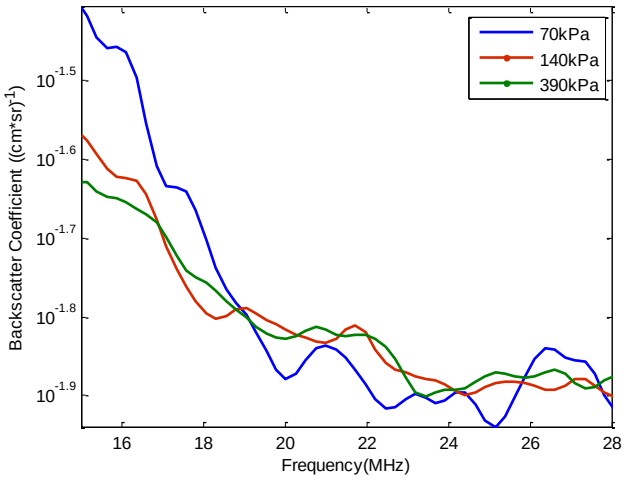

(c)

Figure 4.11 Experimental BSC estimates of UCAs in degassed water for varying incident PRP amplitudes and concentrations of (a) 1x, (b) 2x, and (c) 5x dosage

Estimates of UCA concentration were obtained for at least four trials for each of the 1x, 2x, and 5x concentrations used in the experiments with UCAs in degassed water. These estimates are given in Table 4.3 and were acquired from the experimental BSCs using the Levenberg-Marquardt regression algorithm outlined in Section 3.4.4

Table 4.3 UCA concentration estimates in degassed water acquired with the hemacytometer and using the Levenberg-Marquardt regression from BSCs obtained using a PRP amplitude of 140 kPa

1x Concentration				
Hemacytometer Based Concentration (UCAs/mL)	2.1 ± 0.7E+06	1.8 ± 0.4E+06	1.7 ± 0.4E+06	1.1 ± 3.4E+06
Estimated Concentration (UCAs/mL)	2.5E+06	2.1E+06	2.1E+06	1.1E+06
Elapsed Time to Converge (s)	0.35	0.41	0.44	0.31
2x Concentration				
Hemacytometer Based Concentration (UCAs/mL)	4.6 ± 0.5E+06	4.3 ± 1.3E+06	3.3 ± 0.7E+06	3.3 ± 1.0E+06
Estimated Concentration (UCAs/mL)	4.7E+06	3.7E+06	3.6E+06	3.2E+06
Elapsed Time to Converge (s)	0.32	0.12	0.55	0.51
5x Concentration				
Hemacytometer Based Concentration (UCAs/mL)	8.2 ± 1.3E+06	7.1 ± 1.1E+06	6.7 ± 1.6E+06	1.0 ± 0.4E+07
Estimated Concentration (UCAs/mL)	8.4E+06	6.1E+06	7.4E+06	1.2E+07
Elapsed Time to Converge (s)	0.42	0.35	0.42	0.61

The hemacytometer based estimates were included for comparison and to determine the accuracy of the ultrasonic based UCA concentration estimation technique. They are reported with the average and standard deviation of the six hemacytometer based concentration estimates that were acquired for each trial. All of the ultrasonic based estimates in this table were obtained using the backscatter from UCAs excited with a PRP amplitude of 140 kPa because this was the PRP that gave the optimal estimates compared to the hemacytometer based estimates. The UCA concentration estimates reported in Table 4.3 were all within one standard deviation of the hemacytometer based estimates. In order to determine the effects of PRP amplitude on the UCA concentration estimates, estimates were acquired from BSCs obtained using various PRP amplitudes. For simplicity, only a single trial from each of the 1x, 2x, and 5x concentrations is reported in Table 4.4 for varying PRP amplitude. Although the ultrasonic based estimates of UCA concentration differed for varying PRP amplitudes, they were still within one standard deviation of the hemacytometer based estimates when using PRPs between 140-390 kPa.

4.4.3 UCAs in blood

Estimates of the attenuation coefficient through blood and the BSC of blood were acquired for comparison to previous work and to the theoretical calculations. Because blood has pulsatile value *in vivo*, it was valuable to compare the estimates of attenuation coefficient based upon the flow system data to previous studies performed for varying shear rates. Franceschini et al. [54] estimated whole blood attenuation at 40% hematocrit for shear rates of 5-50 s^{-1}. Their results are shown in Table 4.5.

Table 4.4 UCA concentration estimates in degassed water acquired with the hemacytometer and using the Levenberg-Marquardt regression from BSCs obtained using varying PRP amplitudes

1x Concentration			
Hemacytometer Based Concentration (UCAs/mL)		2.1 ± 0.7E+06	
PRP (kPa)	70	140	390
Estimated Concentration (UCAs/mL)	2.8E+06	2.5E+06	1.5E+06
2x Concentration			
Hemacytometer Based Concentration (UCAs/mL)		4.6 ± 0.5E+06	
PRP (kPa)	70	140	390
Estimated Concentration (UCAs/mL)	5.2E+06	4.7E+06	4.3E+06
5x Concentration			
Hemacytometer Based Concentration (UCAs/mL)		8.2 ± 1.3E+06	
PRP (kPa)	70	140	390
Estimated Concentration (UCAs/mL)	8.1E+06	8.4E+06	7.0E+06

Table 4.5 Estimated attenuation coefficient of porcine whole blood at 40% hematocrit for varying shear rates [54]

Shear Rate (s^{-1})	5	10	20	30	50
Attenuation Coefficent (dB/cm/MHz)	0.053 ± 0.011	0.036 ± 0.008	0.024 ± 0.005	0.016 ± 0.003	0.015 ± 0.003

The estimated attenuation coefficients obtained from the flow system experiments are shown in Figure 4.12. The attenuation was again estimated for varying PRP, and based upon a flow rate of 350 mL/min. The figure also contains the attenuation for the four lowest shear rates reported in Table 4.5 because their slopes more closely matched the experimental data.

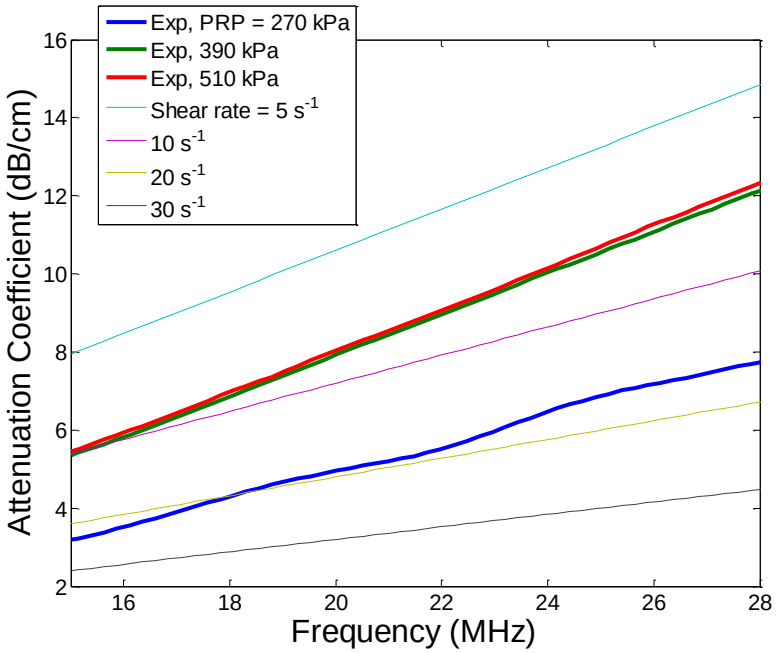

Figure 4.12 Estimated attenuation coefficient of blood using the flow system for varying PRP amplitudes, and previous estimated attenuation [54] for varying shear rates

The slope of the attenuation estimate through blood acquired with an incident PRP amplitude of 270 kPa was slightly lower than the estimates acquired with incident PRP amplitudes of 390 kPa and 510 kPa. Also, the attenuation slope estimate obtained with higher PRP amplitudes and the flow system was similar to the attenuation slope reported in the literature for a shear rate of 5 s^{-1}. However, the magnitude of the attenuation coefficient was different.

The experimental estimates of attenuation through blood were used to estimate the BSC of the blood. Based upon the calculation of theoretical BSCs of blood, the results from these initial experiments were compared to theoretical BSCs without aggregation (the aggregate diameter was set to zero in Equation 2.12). During the experiments, the signal-to-noise ratio (SNR) was noticeably low, even for the highest PRP amplitude of 510 kPa. As a result, when the noise spectrum was subtracted from the mean backscattered power spectrum of the blood, the resulting signal was close to

zero and even negative in some places. Figure 4.13 shows the results of the BSC estimate of blood for varying PRP amplitude, with the negative values missing. The figure also contains the theoretical BSC of blood based upon Equation 2.11 for three hematocrits. Note that if the aggregate diameter in the equation were increased above zero, the slope of the resulting theoretical BSC would decrease, which did not match qualitatively with the experimental BSC estimate.

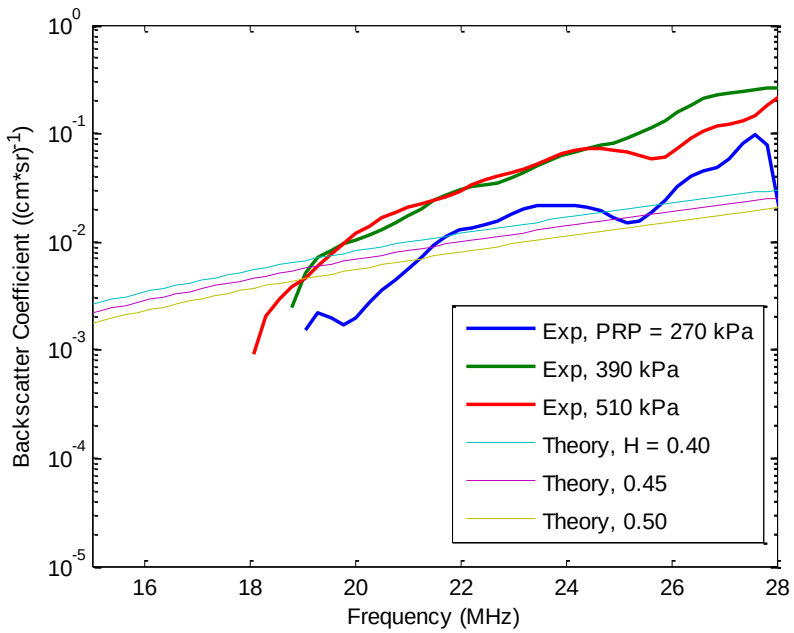

Figure 4.13 Experimental estimates of blood BSC for varying PRP amplitudes, and theoretical calculation of BSC for varying hematocrits (H), reported as a ratio, and for an aggregate diameter of zero

After UCAs were added to the blood, estimates of the BSC were acquired using both the experimentally obtained BSC of blood and the theoretical calculation for blood BSC as references. Attenuation through the UCAs in blood was also estimated using the experimentally acquired attenuation estimates for blood as a reference. The results for attenuation are presented in Figure 4.14.

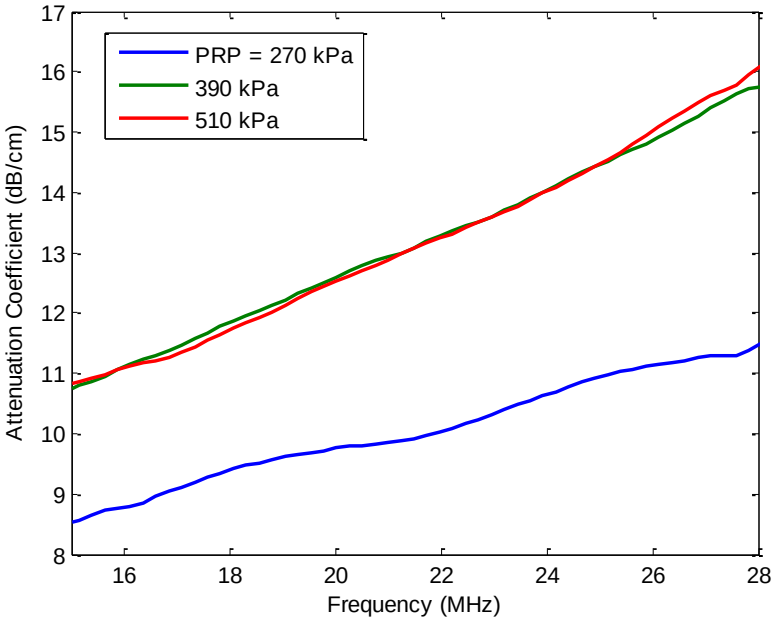

Figure 4.14 UCA attenuation coefficient estimates using the flow system and the experimental attenuation coefficients through blood as references for varying PRP amplitude and a 2x concentration of UCAs

The two BSC estimates, based upon both the experimental and theoretical blood BSC references, are shown in Figure 4.15. The sections where the estimated BSC was negative due to poor SNR are not included in the figure. Because neither of these estimates matched qualitatively with the predictions of the linear model, these results were not used to acquire attenuation estimates. Also, these estimates of attenuation and BSC were based upon initial results from two trials. Therefore, the work with UCAs in blood has only been a preliminary study. Further work is required to improve experimental techniques and acquire accurate estimates.

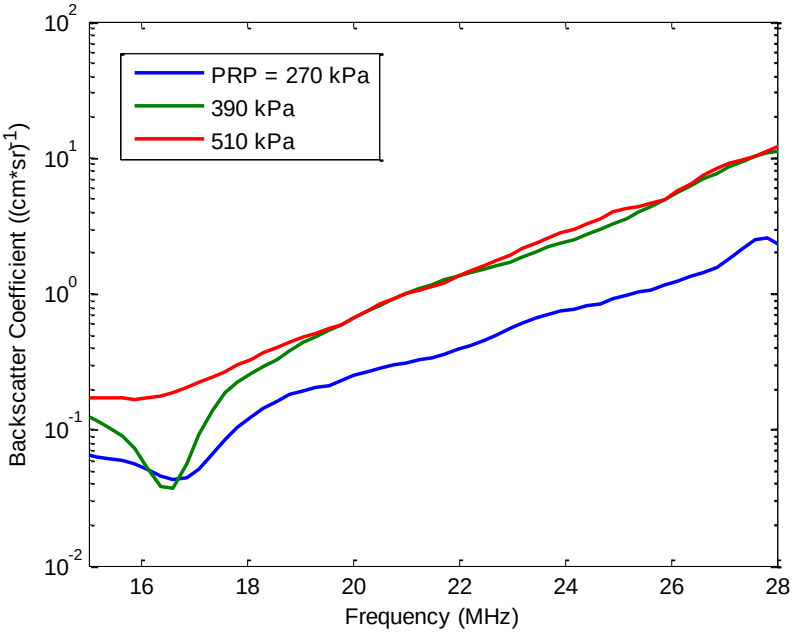

(a)

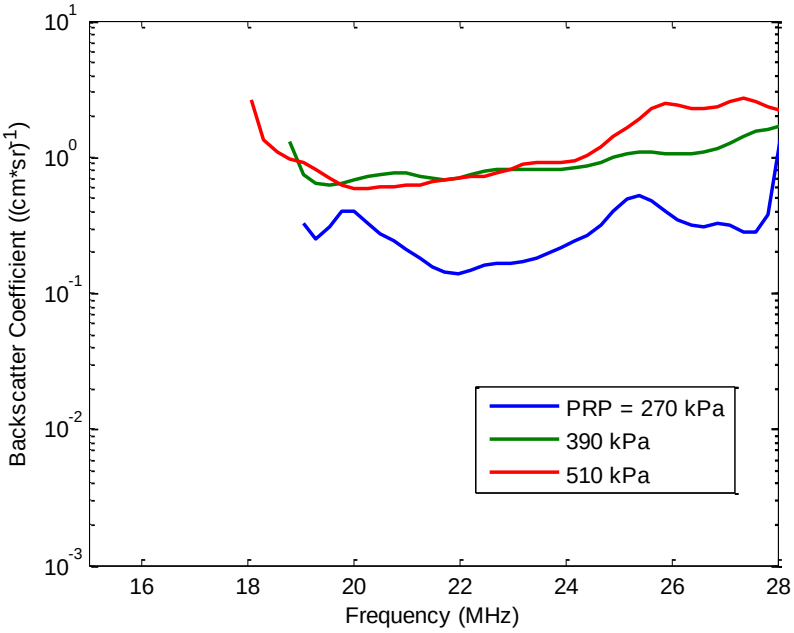

(b)

Figure 4.15 Estimated BSC of UCAs at a 2x concentration in blood for varying PRP amplitude, using blood as a reference medium, and where (a) the experimental BSC of blood was used as the reference BSC or (b) the theoretical BSC of blood was used as the reference BSC

4.5 Results for the simulations of the BSC

It was desirable to examine the behavior of the nonlinear (Marmottant) model at frequencies close to 20 MHz. To do this, the BSC for a volume of randomly located UCAs was simulated with the nonlinear model, as outlined in Chapter 3.5. The input parameters for the simulation were based upon the results from the Levenberg-Marquardt algorithm used to fit the experimental BSCs of UCAs in degassed water to the linear (de Jong) model. More specifically, these parameters were estimates of the mean UCA diameter, standard deviation in diameter, and the UCA concentration. Also, the incident PRP amplitude used was 140 kPa because the UCA concentrations obtained from the experimental BSCs corresponding to this PRP most closely matched the hemacytometer based concentration estimates. Figure 4.16 contains the results of the simulated BSCs (Marmottant model) for an incident PRP amplitude of 140 kPa and 1x, 2x, and 5x concentrations of UCAs, as well as the experimental BSCs for each of those cases and the corresponding theoretical curve predicted by the linear (de Jong) model. The experimental BSCs for an incident PRP amplitude of 140 kPa were used for comparison to the results from the two models.

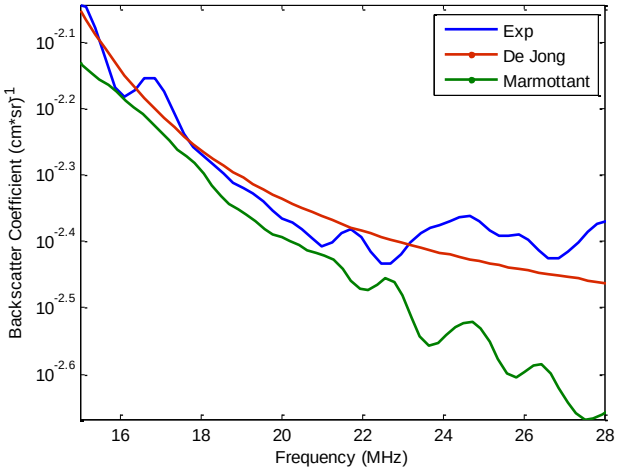

(a)

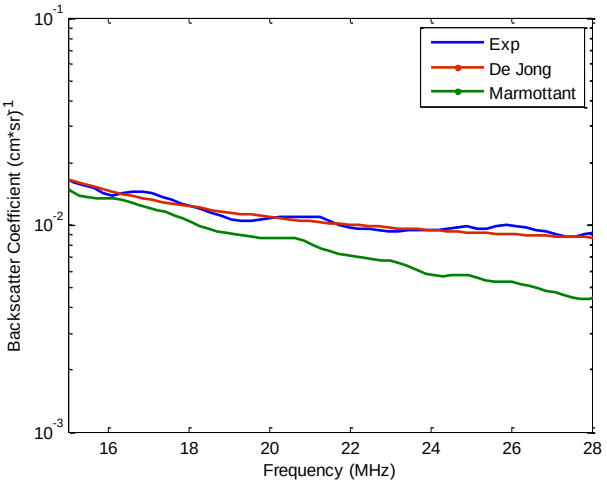

(b)

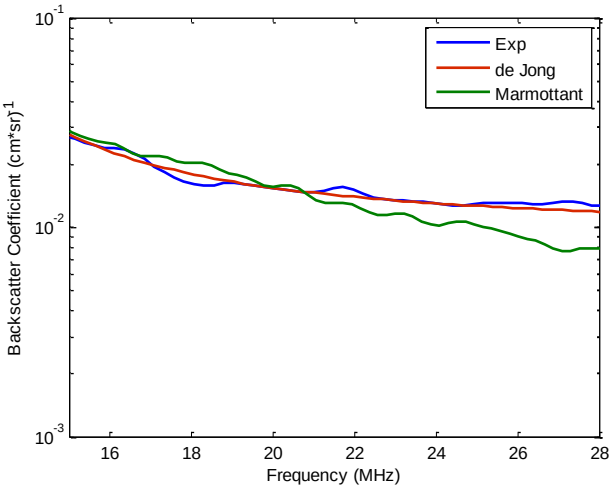

(c)

Figure 4.16 Comparison of the two theoretical models for UCA dynamic with the experimental BSC estimate using an initial PRP of 140 kPa, and an UCA concentration of (a) 1x, (b) 2x, and (c) 5x

CHAPTER 5 DISCUSSION AND FUTURE WORK

5.1 Introduction

In this chapter the results of the four conducted experiments are reviewed and discussed in more detail. Then, a brief discussion of the simulation results is included, and the implications of the results are analyzed in terms of the scattering models that were studied in this work. Finally, the results are summarized and a recommendation for further investigations is highlighted.

5.2 Discussion of experimental results

5.2.1 Beaker experiments

The BSCs in Figure 4.7 vary as a function of depth, indicating a change in the concentration of scatterers. A gradient of concentration was established with respect to height inside the beaker, which was most likely due to the Plexiglas reflector interfering with mixing and the natural buoyancy of the bubbles. This not only affected the backscatter measurements acquired from the vertically positioned transducer, but it also greatly increased the uncertainty of the hemacytometer based concentration estimates. One of the problems with the beaker apparatus, as shown in Figure 3.5, was that the hole for insertion and withdrawal of UCAs and degassed water was located away from the site from which ultrasonic backscatter data was acquired. This made it possible to obtain only an average estimate of concentration in the beaker with the hemacytometer. Therefore, the ultrasonic based UCA concentration estimates in Table 4.1 were only comparable to the hemacytometer based estimates to within an order of magnitude.

As a result of the design weaknesses of the beaker chamber, the flow system was developed. This provided better control of the flow of UCAs across the target site. It also allowed for more efficient withdrawal of a sample of UCAs near the actual ultrasound measurement site in order to provide accurate confirmation of UCA concentration values.

5.2.2 Flow system experiments

5.2.2.1 Glass beads in degassed water

The experimental BSC from the glass beads matched the curve predicted by Faran theory qualitatively between 18 and 28 MHz. These results demonstrated that the flow system and the procedure for estimating BSC could be used to make accurate size and concentration estimates. For all trials, the ESD estimates were within 2% of 49.5 μm, the mean estimated diameter of the beads acquired from the microscope images. Also, because the ESC estimates were no more than 4% different from the glass bead concentration estimates acquired using the water evaporation technique outlined in Section 3.4.3.2, the flow system setup was demonstrated to be robust for estimating multiple concentrations.

When the bead concentration estimates acquired with the water evaporation technique were compared to the average estimate based upon the 5 or 10 g of beads inserted into the beaker, the water evaporation technique produced estimates that were consistently about 20% less than the total concentration of beads in the beaker. This indicated that fewer beads were consistently moving through the flow chamber than were actually inside the beaker reservoir. This result was useful when the experiments with UCAs in degassed water were designed for the flow system; that is, the

hemacytometer based estimates of concentration used for these experiments were better for verifying the concentration in the flow chamber because these estimates were more accurate than estimates based upon the amount inserted (1x, 2x, or 5x concentrations).

The glass beads were used to determine not only whether the concentration in the flow chamber matched the ultrasonic estimates, but also to determine whether the concentration was uniform across the channel inside the flow chamber. If more scatterers in the chamber were to travel down the middle than the sides, the magnitude of the BSC, and subsequently the estimate of concentration, would change as the transducer was moved laterally across the scanning window. This would make it much more difficult to obtain hemacytometer based concentration estimates for the UCAs because the focus of the transducer may not have been directly in line with the location where the degassed water and UCA mixture was extracted. To determine if this was occurring, the focus of the transducer was moved laterally across the scanning window and the corresponding BSC and ESC for the glass beads was estimated. It was found that the maximum difference between ESCs across the entire scanning window was less than 0.5%; therefore, it was concluded that the flow was approximately uniform across the channel.

5.2.2.2 UCAs in degassed water

Many studies [22], [32], [60] have shown that the attenuation of a polydisperse volume of UCAs peaks near the resonance frequencies of the UCAs and then decreases, which was corroborated by the results in Figure 4.10. One previous study [61] estimated the attenuation coefficient of Definity UCAs for a concentration of 200x

the dosage recommended by the manufacturer. Their estimated attenuation reached 31 dB/cm at 30 MHz, which was much higher than previous attenuation estimates [32]. These very high estimates of attenuation indicate that future work *in vivo* must focus on accurate techniques for attenuation estimation, so that the BSC can be correctly estimated.

The hemacytometer based method for estimating UCA concentration was significantly better than the method used in previous studies [21], [22] where the concentration of UCAs was assumed to be uniform and equal to the amount inserted. However, the hemacytometer based estimates still contained some uncertainty due to the movement of the UCAs inside the syringe after extraction and inside the chamber as well. The buoyancy of the UCAs was noticeable while they were being counted because the focal plane of the microscope had to be adjusted slightly over time to account for rising of the UCAs. As explained in Section 3.4.1, the estimates were repeated six times and were therefore reported with an average and standard deviation in the tables. At 140 kPa, the ultrasonic based UCA concentration estimates matched the hemacytometer based estimates to within one standard deviation for all trials and concentrations (Table 4.3).

A major advantage of the flow system was that the UCAs were more uniformly distributed throughout the system than in the beaker experiments. Also, clustering, which can easily occur when the sticky lipid-shelled Definity UCAs are not continuously mixed, was prevented through constant flow and mixing in the beaker. As a result, the BSC estimates of UCAs in degassed water matched qualitatively well with the predictions of the linear de Jong model. In Figure 4.11, however, the BSCs decreased

with increasing incident PRP amplitude, which was not predicted by the linear model. The decrease in BSC magnitude was most likely due to the effects of nonlinear oscillations of UCAs on the BSC. Using Table 4.4, the limits of incident PRP that still resulted in UCA concentration estimates within one standard deviation of the hemacytometer based concentration estimates were determined to be about 140-390 kPa. The BSCs in Figure 4.11 were for PRP amplitudes under 400 kPa. However, the experimental BSCs acquired using PRP amplitudes higher than 400 kPa were also investigated. Figure 5.1 shows the attenuation-compensated, estimated BSC for a concentration of 5x the recommended dosage and a PRP amplitude of 520 kPa.

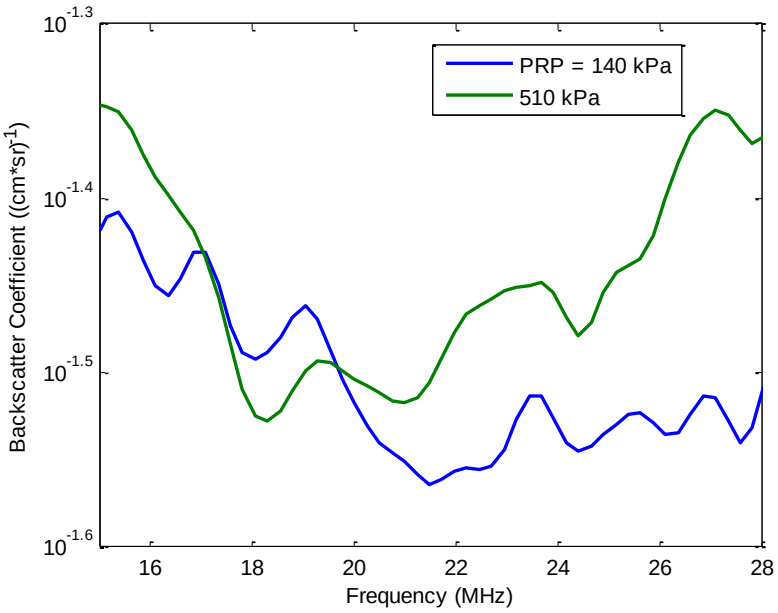

Figure 5.1 Estimated BSC of UCAs in degassed water for two PRPs and a concentration of 5x the recommended dosage

For higher PRP amplitudes and concentrations, the BSC curve began to rise at approximately 22-25 MHz. This behavior was observed for all trials with these parameters. A possible explanation for this is as follows. The majority of UCAs have resonant frequencies of 6-12 MHz, based upon the estimated size distribution and the

predictions for resonant frequencies of the two models in Figure 2.1 and Figure 2.2. Because the 20 MHz pulse from the transducer that was used had a wide bandwidth, some of the smaller UCAs with resonant frequencies of about 12 MHz were excited at resonance. For substantially high PRP and concentrations of these UCAs, their nonlinear oscillations could have produced a strong signal at approximately 25 MHz, the second harmonic of their resonant frequency. This would produce an increase in the scattered power at 25 MHz, which was observed in these cases. Currently, no model that has predicted this behavior is known to the author. In order to avoid bias toward higher UCA concentration estimates due to the increasing BSC above 25 MHz, all of the concentration estimates that were acquired from the estimated BSCs were obtained using a frequency range of 15-25 MHz.

The following novel contributions were made as a result of the experiments with UCAs in degassed water and the flow system. First, a technique for estimating UCA concentration, based upon a Levenberg-Marquardt regression algorithm, was developed to minimize the root mean square error between the linear theoretical model and the experimental BSC estimates. Second, the optimal range for estimating the UCA concentration was determined using the physical properties of the UCA Definity and the predictions of the linear scattering model. Third, the ultrasonic based UCA concentration estimates were verified using a hemacytometer and a sample of the UCA and degassed water mixture that was extracted directly from the chamber where the ultrasonic data was collected. This provided more accurate estimates of UCA concentration than if the amount inserted into the system was assumed to be correct. Lastly, the importance of

restricting the incident PRP amplitude at the target site was demonstrated by acquiring concentration estimates for varying PRP amplitude.

It is important to note two significant constraints to this technique for estimating UCA concentration. First, the frequency range of the BSC from which the concentration estimates were extracted was based upon the calculations of theoretical BSC presented in Section 2.3.1 and was derived using the properties of Definity UCAs. Other commonly used UCAs, which are made of different shell and gas combinations, often have mean diameters that are lower than the mean diameter of Definity UCAs. Because larger UCAs tend to have lower resonance frequencies, a lower frequency range than the 15-25 MHz used for Definity may be more practical. Also, shell properties can significantly affect the resonance frequencies, and so the calculation of theoretical BSCs is necessary for determining an optimal frequency range. The second constraint of the UCA concentration estimation technique is due to the convergence of the Levenberg-Marquardt algorithm. As detailed in Section 3.4.4, the limitations of the estimation technique are due to the three initial parameters, which are the variables that were estimated by the algorithm. The two size distribution parameters did not limit the convergence of the algorithm as long as the initial estimates were within the limits of the size distribution parameter estimates for Definity. However, the algorithm could not converge when the initial UCA concentration was greater than 100 times different than the final value. As a result, if future experiments were conducted with concentrations 100 times greater than the 1x dosage, it would be necessary to have some knowledge of the final concentration in order for the algorithm to converge. This must be

considered when investigations are conducted *in vivo*, where concentrations can vary greatly among target locations.

5.2.2.3 UCAs in blood

Attenuation estimates that were acquired with the flow system for higher PRP amplitudes did match previous estimates for attenuation slope in the literature at a shear rate of 5 s^{-1}. However, two observations were made. First, although the slope of the attenuation coefficient matched previous results, the magnitude of the attenuation was lower. A possible explanation for this is that the previous estimates of attenuation in whole blood were based upon a hematocrit of 40%. Although the hematocrit was not determined for the blood samples used in the flow system experiments, it is possible that a different blood hematocrit was used, which could correspond to a different magnitude of the attenuation coefficient. The second observation was that the attenuation estimate acquired with a PRP amplitude of 270 kPa was lower in magnitude than the estimates acquired with higher PRPs, and the estimate matched the slope of the estimates in the literature for faster shear rates. During the experiments with blood in the flow system, a higher level of noise was observed. The SNR of the data acquired with a PRP of 270 kPa was lower than the SNR of the data acquired with higher PRPs. This may have resulted in an inaccurate estimate for the lower PRP. Also, the attenuation estimates reported in the literature were assumed to be linear with frequency and averaged over many trials. This could have created a bias toward linear estimates of attenuation because the data was fit to a linear model.

The estimates for the BSC of blood reported in Figure 4.13 reflect the low SNR that affected the data for all PRP amplitudes. Below 18 MHz, the power spectra of the

blood backscatter were below the noise floor; therefore, the BSCs were only reported above 18 MHz. The overall slope of the estimated BSCs was greater than that predicted by the theoretical model for blood BSC, even when the aggregation of blood was ignored. When the hematocrit was increased, the theoretical BSC decreased. It was therefore likely that the porcine whole blood that was used had a lower hematocrit.

When the attenuation estimates of the UCAs, using blood as the reference, were compared to those acquired in water, the results were quite different. The magnitude of the estimated attenuation of UCAs in blood was almost double the magnitude of the estimates for UCAs in water. Also, for UCAs in blood, the attenuation estimates increased with increasing frequency. These estimates do not match those obtained for UCAs in previous studies, as do the estimates acquired from UCAs in water. Finally, the attenuation estimates for UCAs were approximately the same for a PRP amplitude of 390 kPa and 510 kPa. This does not agree with the experimental results or with previous studies [32]. The attenuation estimate acquired with a PRP amplitude of 270 kPa was the lowest estimate, which was consistent with the results from the experiments with UCAs in degassed water. However, this could have been because the experimental attenuation estimate for blood using a PRP amplitude of 270 kPa was lower than the estimates for blood with higher PRP amplitudes. Therefore, the attenuation estimates will need to be repeated more carefully in the future in order to acquire accurate estimates.

The estimates of the BSC of UCAs in blood did not match qualitatively with the theoretical predictions for the BSC of UCAs with the linear model. The estimated BSC that was obtained using the experimental BSC of blood as a reference had a large

positive slope with respect to frequency, rather than the small negative slope predicted by the model. As a result, the linear scattering model for UCAs was not used to extract concentration estimates. Also, hemacytometer based estimates of UCA concentration in blood could not be obtained. The RBCs covered the UCAs and made it difficult to see and count the UCAs under the microscope. In the future, alternative methods for verifying UCA concentrations in blood must be devised.

The overall magnitude of the BSC estimates of UCAs in blood was much greater than the magnitude of the BSC estimates for the same 2x concentration of UCAs in water. One possible explanation for the large positive slope and magnitude difference is the way the estimate of BSC was calculated. In order to obtain the BSC, the ratio of the backscattered power from UCAs in blood to the backscattered power from blood alone was computed. However, the backscattered power from the blood alone had a very poor SNR, as evidenced by the negative values in the power spectrum after the noise spectrum was subtracted and the resulting experimental BSC estimates for blood. If the power spectrum from the blood alone was mostly due to averaging of noise fluctuations, computing the ratio of the power spectra was equivalent to dividing the power spectrum from UCAs in blood by low magnitude values and noise. This amplified the magnitude of the noise, causing the estimate of BSC to be inaccurate and large in magnitude. Before the estimates for the BSC of UCAs in blood can be used to extract UCA concentration estimates, methods to improve the estimation of the power spectrum from blood and the corresponding SNR need to be devised.

The procedure used to estimate the BSC of UCAs in blood was based upon the assumption that the backscattered power from UCAs alone is much greater than the

backscattered power from blood alone. To examine the validity of this assumption, previous results for BSCs of porcine whole blood [46], as well as the results for blood BSC estimates obtained in the flow system experiments, were compared to the results obtained for the BSC of UCAs in degassed water. The BSC of porcine whole blood [46] with a 40% hematocrit is shown in Figure 5.2.

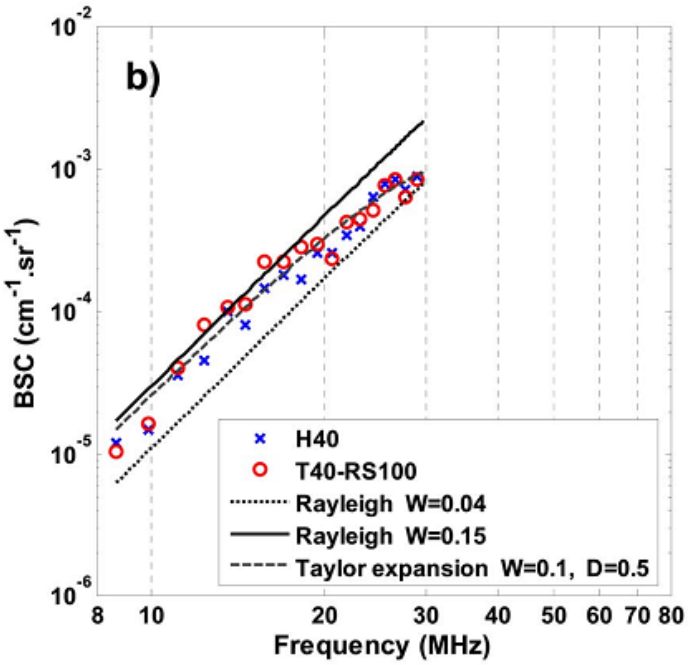

Figure 5.2 From [46], the estimated BSC for porcine whole blood at 40% hematocrit (H40), 40% hematocrit and a shear rate of 100 s^{-1} (T40-RS100), and the predictions of their theoretical model

The BSC was approximately $10^{-3.1}$ 1/cm/sr in [46] and 10^{-1} 1/cm/sr at 25 MHz. By contrast, the BSC of UCAs at a concentration of 1x is approximately $10^{-2.1}$ at 25 MHz. Using the results from [46], the BSC of UCAs was greater than ten times the BSC of blood alone in the frequency range of 15-25 MHz. Therefore, the assumption is valid. However, if the estimates of the BSC of blood from the flow system experiments are accurate (Figure 4.15), the assumption is no longer valid. Future work must focus on

better estimation of the BSC of blood in order to determine if the assumption is valid for the frequency range of 15-25 MHz.

A few more suggestions for future work with this technique for estimating UCA concentration in blood are provided. First, the most significant reason for the inaccurate estimates of attenuation and BSC of UCAs in blood was the poor SNR that was achieved for the PRP amplitudes that were used. Because this technique for estimating UCA concentration requires low PRP amplitudes for the linear model to be used to acquire estimates, it will be necessary to maintain *in situ* PRP amplitudes of at most 510 kPa in future work. Therefore, other techniques for increasing the SNR without increasing the PRP amplitude must be explored. Also, the hemacytometer was not fit for extracting optical estimates of UCA concentration in blood, as reported above. Therefore, a technique for verifying ultrasound based UCA concentration estimates must be developed. Finally, a method for obtaining the hematocrit of the blood samples that were used will need to be implemented.

5.3 Discussion of the simulation and scattering models

Referring to Figure 4.16, the nonlinear Marmottant model did not predict the shape of the experimental BSC for a PRP of 140 kPa and frequencies above 20 MHz. The slope of the simulated BSC based upon the Marmottant model was more negative than that of the experimental BSC and corresponding theoretical predictions of the linear model. Although the BSCs were similar for lower frequencies, which were closer to the resonance frequencies of most of the UCAs, the magnitude of the backscattered power from the oscillating UCAs in the simulation decreased significantly above 20 MHz.

It is hypothesized that for the properties of Definity and the simulated experimental conditions, the scattered power from UCAs excited above 20 MHz is dominated by the size of the UCAs rather than their movement. Therefore, the Marmottant model would be better for predicting the scattered power from UCAs oscillating with large amplitudes close to their resonance frequencies, and the linearized de Jong model would be more suitable for predicting the BSC when an UCA is excited at frequencies much higher than its resonance frequency. Another possible explanation for the lack of agreement between the simulated and experimental data was that the model does not incorporate the effect of frequency dependent shell properties. Goertz et al. [32] observed that the shell dilatational viscosity term, κ_s, for Definity was both frequency and size dependent. In fact, they found that shell viscosity decreased for increasing UCA diameter. Also, they concluded that small Definity UCAs undergo substantially more nonlinear oscillations at higher frequencies than other UCA types of similar size.

One of the caveats of using the linear model was the assumption of linear oscillations. Because the nonlinear Marmottant model, introduced in Section 2.3.2, was designed to predict the occurrence of nonlinear oscillation more accurately than other previously derived nonlinear models, it was used to determine the limit of PRP amplitude above which nonlinear oscillations were present. The scattered pressure from a 2.2-μm UCA was simulated using a 20-MHz Gaussian pulse with a fractional bandwidth of 80%, parameters for Definity, and PRP amplitudes from 5 to 1000 kPa in 5 kPa increments. Three types of results were discovered. First, for PRP amplitudes below 20 kPa, the maximum peak occurred at about 8 MHz, close to the resonance

frequency of the 2.2 μm diameter UCA based upon the Marmottant formulation. Second, for PRP amplitudes between 20 kPa and 65 kPa, the magnitude of the first harmonic at 20 MHz dominated, and no visible second harmonic peaked within 60 dB of the first harmonic. Finally, for PRP amplitudes above 65 kPa, the spectrum contained a visible second harmonic that increased as PRP amplitude increased. Examples of these three cases are shown in Figure 5.3.

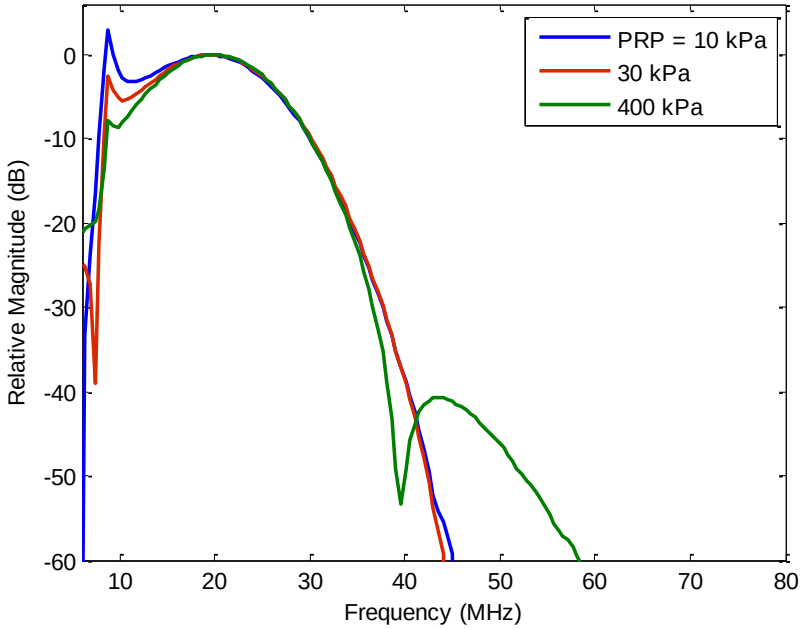

Figure 5.3 Simulation results for scattered pressure from a 2.2-μm UCA excited with a 20 MHz center frequency Gaussian pulse for varying PRP amplitude, normalized to the peak at 20 MHz

For comparison, the PRP amplitudes used in the experiments with UCAs from this work ranged from about 70 to 500 kPa, and the linear model was used to make UCA concentration estimates that were within one standard deviation of the hemacytometer based estimates for all trials using PRP amplitudes of about 140-390 kPa. Although these pressures are above the 65 kPa limit for nonlinear oscillations predicted by the Marmottant model, the magnitude of the second harmonic for an

incident PRP of 400 kPa, calculated using the model, was 40 dB down from the peak at 20 MHz. At this incident PRP level, the magnitude of the scattered pressure due to nonlinear oscillations was one hundredth the scattered pressure from the first harmonic. Therefore, the effects from nonlinear oscillations were not significant enough to cause large deviations from the predictions of the linear model.

The onset of nonlinear oscillations has also been investigated for other UCA types and frequency ranges [35], [62]. De Jong et al. [35] reported that the scattered pressure from coated UCAs has been observed to contain energy in higher harmonics for incident PRP amplitudes as low as 20-50 kPa. They conducted an experiment with Sonovue (Bracco, Milan, Italy) UCAs insonated at 3.5 MHz for varying incident PRP amplitudes. Second harmonic energy was observed above the noise floor for a minimum incident PRP amplitude of 24 kPa. Qin et al. [62], on the other hand, cited a nonlinear model and the experimental work from previous studies and used the predicted radius versus time curves from the model to estimate the onset of nonlinear oscillations. They reported that a 2-μm-diameter UCA insonated at 1 MHz will exhibit nonlinear oscillatory behavior for incident PRPs of at least 150 kPa. However, the results from these previous studies were performed using excitation frequencies less than 10 MHz. No previous work has been done to determine the onset of nonlinear oscillations for excitation frequencies close to 20 MHz.

If the assumption of linear oscillations is no longer valid, UCA concentration estimates using the linear model may be inaccurate. However, nonlinear oscillations are more prevalent when a UCA is excited at or near its resonant frequency. With this technique for estimation of UCA concentration, the UCAs are excited above their

resonant frequencies, and therefore, the pressure threshold above which nonlinear oscillations dominate is higher for these frequencies than for resonant excitation frequencies. As a result, the UCA concentration estimates acquired using the technique presented in this work should remain accurate for higher PRP amplitudes.

5.4 Conclusions

In this work a noninvasive technique for estimating the concentration of UCAs *in vitro* was developed, using a linearized theoretical model for scattering from UCAs. Estimates of UCA concentration in degassed water were obtained by fitting the estimated BSC to the linearized theoretical model in the frequency range of 15-25 MHz. The technique was verified for the experiments in degassed water with hemacytometer based estimates obtained by the withdrawal of the UCA and water mixture from the system. Results indicated that the experimental setup and technique were successful for estimating both glass bead and UCA concentrations in degassed water within the limits of the pressure amplitudes used in the experiments. Ultrasonic based estimates of UCA concentration were within one standard deviation of the hemacytometer based concentration estimates for incident PRP amplitudes of 140-390 kPa.

The results for the four conducted experiments are summarized as follows. UCA concentration estimates acquired from the beaker experiments with UCAs in degassed water showed that UCA concentration varied with depth, such that the concentration of UCAs increased with increasing height in the beaker. Due to this concentration gradient, it was difficult to verify the concentration estimates with the hemacytometer. In order to eliminate this problem, the second and third experiments were conducted in the flow system that was developed. For these experiments, concentration estimates of glass

beads and UCAs in degassed water were obtained by estimating the BSC using pulse/echo ultrasound. The concentration estimates of the glass beads were verified using a water evaporation technique to separate and estimate the mass of beads in the system. Both these estimates of glass bead concentration and the hemacytometer based estimates of UCA concentration indicated that the ultrasound based concentration estimation technique was successful using the flow system with degassed water. Finally, initial experiments were conducted to estimate the BSC of UCAs using blood as a reference medium in the flow system. Results indicated that further work will be required to refine the concentration estimation technique and the verification process so that the technique can be extended to *in vivo* applications.

In order to be able to obtain UCA concentration estimates at a target site *in vivo*, further investigation of the ultrasound based UCA concentration estimation technique is required. The technique depends upon the use of a model for small UCA oscillations, which limits the range of incident PRP amplitudes that can be used to produce accurate results. The ability to estimate the PRP amplitude *in vivo* would ensure the accuracy of the UCA concentration estimates. Further studies could then be used to determine the relationship between the *in vivo* PRP estimates and common clinical parameters such as the mechanical index (MI). For example, one recent study estimated UCA destruction *in vivo* by varying the concentrations of UCAs in µL/kg via bolus injections and by varying the MI within clinical limits [63]. By relating the destruction of UCAs to MI and the concentrations of bolus injections, the authors created a method for estimating UCA destruction that can be easily implemented in the clinic. It is recommended that further studies be conducted to provide guidelines for the UCA concentrations and

common clinical parameters such as MI that can be used to acquire accurate UCA concentration estimates.

One advantage of using the blood itself as a reference *in vivo*, as was outlined for *in vitro* work in Section 3.4.3, is the ability to acquire UCA concentration estimates without the need for estimation of the intervening tissue transmission and attenuation losses. In the *in vitro* work presented here, an insertion loss method was used with a Plexiglas reflector as the reference. The attenuating medium was placed between the ultrasound transducer and the reflector so that the reflected waves could be compared with and without the medium. For *in vivo* work, however, it is not feasible to use this technique due to the need for a plane reflector inside the tissue. Therefore, a new method for estimating the attenuation for each trial is vital to be able to accurately estimate the BSC of UCAs *in vivo*. This could occur through estimating both UCA concentration and attenuation from the backscatter.

Finally, as was emphasized in Section 1.2, the concentrations of UCAs that have been shown to enhance ultrasound based therapeutic techniques are much higher than those currently used for imaging (a 1x concentration of Definity for imaging is about 9.6×10^5 UCAs/mL, as recommended by the manufacturer). The assumption used to derive the BSC with the linear model was that minimal multiple scattering was occurring. This corresponds to a linear relationship between UCA concentration and backscattered power, which was previously found to hold for concentrations up to 2×10^7 UCAs/mL, or about 20 times the recommended concentration for imaging [20]. However, because concentrations may vary by the type of injection and by the type of tissue *in vivo*, it is probable that UCA clouds with very high concentrations will be present in some

locations. Effects of UCA interactions cannot be neglected for these high concentrations, as was done for the derivation of the BSC with the linear model in this work. In fact, one study found that the pressure threshold for UCA destruction increased significantly for very high UCA concentrations [64]. Therefore, an *in vivo* implementation of the UCA concentration estimation technique would require further studies of the relationship between backscattered power and UCA clouds with higher concentrations to include the effects of multiple scattering and possible UCA interactions. Each of these suggestions for further investigation will be useful for the extraction of UCA concentration estimates to be extended to *in vivo* applications.

REFERENCES

[1] M. Averkiou, J. Powers, D. Skyba, M. Bruce, and S. Jensen, “Ultrasound contrast imaging research,” *Ultrasound Quarterly*, vol. 19, pp. 27-37, 2003.

[2] D. Cosgrove and C. Harvey, “Clinical uses of microbubbles in diagnosis and treatment,” *Medical and Biological Engineering and Computing*, vol. 47, pp. 813-826, 2009.

[3] H. Becker and P. Burns, *Handbook of Contrast Echocardiography,* Heidelberg, Germany: Springer-Verlag, 2000, pp. 82-83.

[4] D. L. Miller and C. Dou, “Membrane damage thresholds for pulsed or continuous ultrasound in phagocytic cells loaded with contrast agent gas bodies,” *Ultrasound in Medicine and Biology*, vol. 30, pp. 405-411, 2004.

[5] D. L. Miller, C. Dou, and R. C. Wiggins, “Frequency dependence of kidney injury induced by contrast-aided diagnostic ultrasound in rats,” *Ultrasound in Medicine and Biology*, vol. 34, pp. 1678-1687, 2008.

[6] D. M. Skyba R. J. Price, A. Z. Linka, T. C. Skalak, and S. Kaul, “Direct *in vivo* visualization of intravascular destruction of microbubbles by ultrasound and its local effects on tissue,” *Circulation*, vol. 98, pp. 290-293, 1998.

[7] R. Bekeredjian, P. A. Grayburn, and R. V. Shohet, “Use of ultrasound contrast agents for gene or drug delivery in cardiovascular medicine,” *Journal of the American College of Cardiology*, vol. 45, pp. 329-225, 2005.

[8] Z. Fan, R. E. Kumon, J. Park, and C. X. Deng, “Intracellular delivery and calcium transients generated in sonoporation facilitated by microbubbles,” *Journal of Controlled Release*, vol. 142, pp. 31-39, 2010.

[9] M. M. Forbes, R. L. Steinberg, and W. D. O'Brien Jr., “Frequency-dependent evaluation of the role of Definity in producing sonoporatior of Chinese hamster ovary cells,” *Journal of Ultrasound in Medicine*, vol. 30, pp. 61-69, 2011.

[10] E. Kimmel, “Cavitation bioeffects,” *Critical Reviews in Biomedical Engineering*, vol. 34, pp. 105-161, 2006.

[11] C. A. Johnson, S. Sarwate, R. J. Miller, and W. D. O’Brien Jr, “A temporal study of ultrasound contrast agent-induced changes in capillary density,” *Journal of Ultrasound in Medicine*, vol. 29, pp. 1267-1275, 2010.

[12] M. R. Bailey et al., “Cavitation detection during shock-wave lithotripsy,” *Ultrasound in Medicine and Biology*, vol. 31, pp. 1245-1256, 2005.

[13] E. P. Stride and C. C. Coussios, “Cavitation and contrast: The use of bubbles in ultrasound imaging and therapy,” *Proceedings of the Institution of Mechanical Engineers, Part H: Journal of Engineering in Medicine*, vol. 224, pp. 171-191, 2010.

[14] W. Luo et al., “Ablation of high-intensity focused ultrasound assisted with SonoVue on rabbit VX2 liver tumors: Sequential findings with histopathology, immunohistochemistry, and enzyme histochemistry,” *Annals of Surgical Oncology*, vol. 16, pp. 2359-2368, 2009.

[15] F. Li and L. Fu, “Using microbubble contrast agent of different dosage to enhancing liver ablation induced by high-intensity focused ultrasound,” in *IFMBE Proceedings*, vol. 25, 2009, pp. 39-42.

[16] T. Nishihara, H. Utashiro, M. Ichiyanagi, K. Yoshinaka, S. Takagi, and Y. Matsumoto, “Heating location control of HIFU treatment enhanced with microbubbles contrast agents,” in *IFMBE Proceedings*, vol. 31, 2010, pp. 1397-1400.

[17] D. A. B. Smith et al., “Ultrasound-triggered release of recombinant tissue-type plasminogen activator from echogenic liposomes,” *Ultrasound in Medicine and Biology*, vol. 36, pp. 145-157, 2010.

[18] J. R. Eisenbrey, M. C. Soulen, and M. A. Wheatley, “Delivery of encapsulated doxorubicin by ultrasound-mediated size reduction of drug-loaded polymer contrast agents,” *IEEE Transactions on Biomedical Engineering*, vol. 57, pp. 24-28, 2010.

[19] D. W. Droste. “Clinical utility of contrast-enhanced ultrasound in neurosonology.” *European Neurology*, vol. 59, pp. 2-8, 2008.

[20] M. Lampaskis and M. Averkiou, “Investigation of the relationship of nonlinear backscattered ultrasound intensity with microbubble concentration at low MI,” *Ultrasound in Medicine and Biology*, vol. 36, pp. 306-312, 2010.

[21] C. M. Moran, R. J. Watson, K. A. A. Fox, and W. N. McDicken, “*In vitro* acoustic characterization of four intravenous ultrasound contrast agents at 30 MHz,” *Ultrasound in Medicine and Biology*, vol. 28, pp. 785-791, 2002.

[22] J. N. Marsh et al. “Frequency and concentration dependence of the backscatter coefficient of the ultrasound contrast agent Albunex,” *Journal of the Acoustical Society of America*, vol. 104, pp. 1654-1666, 1998.

[23] J. J. Faran, “Sound scattering by solid cylinders and spheres,” *Journal of the Acoustical Society of America*, vol. 24, pp. 405-418, 1951.

[24] M. F. Insana and T. J. Hall, “Parametric ultrasound imaging from backscatter coefficient measurements: image formation and interpretation,” *Ultrasonic Imaging*, vol. 12, pp. 245-267, 1990.

[25] R. J. Lavarello, G. Ghoshal, and M. L. Oelze, “On the estimation of backscatter coefficients using single element focused transducers,” *Journal of the Acoustical Society of America*, vol. 129, pp. 2903-2911, 2011.

[26] R. S. C. Cobbold, *Foundations of Biomedical Ultrasound*, Oxford, UK: Oxford University Press, 2006.

[27] R. Wildt, “Acoustic theory of bubbles,” US Navy, *Physics of Sound in the Sea*, NDRC Summary, Technical Report Division 6, vol. 8, 1946.

[28] N. de Jong, L. Hoff, T. Skotland, and N. Bom, “Absorption and scatter of encapsulated gas filled microspheres: theoretical considerations and some measurements,” *Ultrasonics*, vol 30, pp. 95-103, 1992.

[29] H. Medwin, “Counting bubbles acoustically: a review,” *Ultrasonics*, vol. 15, pp. 7-13, 1977.

[30] N. de Jong and L. Hoff, “Ultrasound scattering properties of Albunex microspheres,” *Ultrasonics*, vol. 31, pp. 175-181, 1993.

[31] J. Gorce, M. Arditi, and M. Schneider, “Influence of bubble size distribution on the echogenicity of ultrasound contrast agents: a study of Sonovue™,” *Investigative Radiology*, vol. 35, pp. 661-671, 2000.

[32] D. E. Goertz, N. de Jong, and A.F. van der Steen, “Attenuation and size distribution measurements of Definity and manipulated Definity populations,” *Ultrasound in Medicine and Biology*, vol. 33, pp. 1376-1388, 2007.

[33] T. Faez, D. Goertz, and N. de Jong, “Characterization of Definity ultrasound contrast agent at frequency range of 5-15 MHz,” *Ultrasound in Medicine and Biology*, vol. 37, pp. 338-342, 2010.

[34] P. Marmottant et al., “A model for large amplitude oscillations of coated bubbles accounting for buckling and rupture,” *Journal of the Acoustical Society of America*, vol. 118, pp. 3499-3505, 2005.

[35] N. de Jong, M. Emmer, A. van Wamel, and M. Versluis, “Ultrasonic characterization of ultrasound contrast agents,” *Medical and Biological Engineering and Computing*, vol. 47, pp. 861-873, 2009.

[36] D. A. King and W. D. O'Brien Jr., "Comparison between maximum radial expansion of ultrasound contrast agents and experimental postexcitation signal results," *Journal of the Acoustical Society of America*, vol 129, 114-121, 2011.

[37] M. Overvelde et al. "Nonlinear shell behavior of phospholipid-coated microbubbles," *Ultrasound in Medicine and Biology*, vol. 36, pp. 2080-2092, 2010.

[38] J. Sijl et al., "Acoustic characterization of single ultrasound contrast agent microbubbles," *Journal of the Acoustical Society of America*, vol. 124, pp. 4091-4097, 2008.

[39] J. Sijl et al., "Subharmonic behavior of phospholipid-coated ultrasound contrast agent microbubbles," *Journal of the Acoustical Society of America*, vol. 128, pp. 3239-3252, 2010.

[40] K. K. Shung, R. A. Sigelmann, and J. M. Reid, "Scattering of ultrasound by blood," *IEEE Transactions on Biomedical Engineering*, vol. 23, pp. 460-467, 1967.

[41] C. Coussios, "The significance of shape and orientation in single-particle weak-scatterer models," *Journal of the Acoustical Society of America*, vol. 112, pp. 906-915, 2002.

[42] D. Savéry and G. Cloutier, "High-frequency ultrasound backscattering by blood: analytical and semianalytical models of the erythrocyte cross section," *Journal of the Acoustical Society of America*, vol. 121, pp. 3963-3971, 2007.

[43] S. Wang and K. K. Shung, "An approach for measuring ultrasonic backscattering from biological tissues with focused transducers," *IEEE Transactions on Biomedical Engineering*, vol. 44, pp. 549-554, 1997.

[44] L. Mo, I-Y. Kuo, K. K. Shung, L. Ceresne, and R. S. C. Cobbold, "Ultrasound scattering from blood with hematocrits up to 100%," *IEEE Transactions on Biomedical Engineering*, vol. 41, pp. 91-95.

[45] E. Franceschini, F. T. H. Yu, and G. Cloutier, "Simultaneous estimation of attenuation and structure parameters of aggregated red blood cells from backscatter measurements," *Journal of the Acoustical Society of America: Express Letters*, vol. 123, pp. EL85-EL91, 2008.

[46] F. T. H. Yu and G. Cloutier, "Experimental ultrasound characterization of red blood cell aggregation using the structure factor size estimator," *Journal of the Acoustical Society of America*, vol. 122, pp. 645-656, 2007.

[47] M. L. Oelze, W. D. O'Brien Jr., J. P. Blue, and J. F. Zachary, "Differentiation and characterization of rat mammary fibroadenomas and 4T1 mouse carcinomas using quantitative ultrasound imaging," *IEEE Transactions on Medical Imaging*, vol. 23, pp. 764-771, 2004.

[48] M. O'Donnell and J. G. Miller, ''Quantitative broadband ultrasonic backscatter: An approach to nondestructive evaluation in acoustically inhomogeneous materials,'' *Journal of Applied Physics*, vol. 52, pp. 1056–1065, 1981.

[49] M. L. Oelze and W. D. O'Brien Jr., "Frequency dependent attenuation-compensation functions for ultrasonic signals backscattered from random media." *Journal of the Acoustical Society of America*, vol. 111, pp. 2308-2319, 2001.

[50] D. A. King and W. D. O'Brien Jr., "Comparison between maximum radial expansion of ultrasound contrast agents and experimental postexcitation signal results," *Journal of the Acoustical Society of America*, vol. 129, pp. 114-121, 2011.

[51] P. A. Dayton, K. E. Morgan, A. L. Klibanov, G. H. Brandenburger, and K. E. Ferrara, "Optical and acoustical observations of the effects of ultrasound on contrast agents," *IEEE Transactions on Ultrasonics, Ferroelectrics, and Frequency Control*, vol. 46, pp. 220-232, 1999.

[52] A. Haak, R. Lavarello, and W. D. O'Brien Jr., "Semiautomatic detection of microbubble ultrasound contrast agent destruction applied to Definity using support vector machines," in *Proceedings – IEEE Ultrasonics Symposium*, 2007, pp. 660-663.

[53] M. Mleczko and G. Schmitz, "A method for the determination of the inertial cavitation threshold of ultrasound contrast agents," in *Proceedings – IEEE International Ultrasonics Symposium*, 2008, pp.1686-1689.

[54] E. Franceschini, F. T. H. Yu, F. Destrempes, and G. Cloutier, "Ultrasound characterization of red blood cell aggregation with intervening attenuating tissue-mimicking phantoms," *Journal of the Acoustical Society of America*, vol. 127, pp. 1104-115, 2010.

[55] K. Levenberg, "A method for the solution of certain non-linear problems in least squares," *Quarterly of Applied Mathematics*, vol. 2, pp. 164-168, 1944.

[56] D. Marquardt, "An algorithm for least-squares estimation of nonlinear parameters," *SIAM Journal of Applied Mathematics*, vol. 11, pp. 431–441, 1963.

[57] J. A. Jensen and N. B. Svendsen, "Calculation of pressure fields from arbitrarily shaped, apodized, and excited ultrasound transducers," *IEEE Transactions on Ultrasonics, Ferroelectrics, and Frequency Control*, vol. 39, pp. 262-267, 1992.

[58] J. A. Jensen, “A program for simulating ultrasound systems,” in *Proceedings of the 10th Nordic-Baltic Conference on Biomedical Imaging*, 1996, pp. 351-353.

[59] S. Hilgenfeldt, D. Lohse, and M. Zomack, “Response of bubbles to diagnostic ultrasound: a unifying theoretical approach,” *The European Physical Journal B*, vol. 4, pp. 247-255, 1998.

[60] D. Chatterjee, K. Sarkar, P. Jain, and N. E. Schreppler, “On the suitability of broadband attenuation measurement for characterizing contrast agent microbubbles,” *Ultrasound in Medicine and Biology*, vol. 31, pp. 781-786, 2005.

[61] S. Stapleton et al., “Acoustic and kinetic behavior of Definity in mice exposed to high frequency ultrasound,” *Ultrasound in Medicine and Biology*, vol. 35, pp. 296-307, 2009.

[62] S. Qin, C. S. Caskey, and K. W. Ferrara, “Ultrasound contrast microbubbles in imaging and therapy: physical principles and engineering,” *Physics in Medicine and Biology*, vol. 54, pp. R27-R57, 2009.

[63] S.-H. Hung, C.-K. Yeh, T.-H. Tsai, T. Chen, and R.-C. Chen, “A simple method for quantifying ultrasound-triggered microbubble destruction,” *Ultrasound in Medicine and Biology*, vol. 37, pp. 949-957, 2011.

[64] K. Yasui, J. Lee, T. Tuziuti, A. Towata, T. Kozuka, and Y. Lida, “Influence of the bubble-bubble interaction on destruction of encapsulated microbubbles under ultrasound,” *Journal of the Acoustical Society of America*, vol. 126, pp. 973-982, 2009.